

VTT Technical Research Centre of Finland

## Combining Rigid Cellulose Nanocrystals and Soft Silk Proteins

Leppänen, Ilona; Arola, Suvi; King, Alistair W.T.; Unger, Miriam; Stadler, Hartmut; Nissen, Gry Sofie; Zborowski, Charlotte; Virtanen, Tommi; Salmela, Juha; Setälä, Harri; Lésage, Stephanie; Österberg, Monika; Tammelin, Tekla

*Published in:*  
Advanced Materials Interfaces

*DOI:*  
[10.1002/admi.202300162](https://doi.org/10.1002/admi.202300162)

Published: 17/07/2023

*Document Version*  
Publisher's final version

[Link to publication](#)

*Please cite the original version:*

Leppänen, I., Arola, S., King, A. W. T., Unger, M., Stadler, H., Nissen, G. S., Zborowski, C., Virtanen, T., Salmela, J., Setälä, H., Lésage, S., Österberg, M., & Tammelin, T. (2023). Combining Rigid Cellulose Nanocrystals and Soft Silk Proteins: Revealing Interactions and Alignment in Shear. *Advanced Materials Interfaces*, 10(20), Article 2300162. <https://doi.org/10.1002/admi.202300162>



VTT  
<http://www.vtt.fi>  
P.O. box 1000FI-02044 VTT  
Finland

By using VTT's Research Information Portal you are bound by the following Terms & Conditions.

I have read and I understand the following statement:

This document is protected by copyright and other intellectual property rights, and duplication or sale of all or part of any of this document is not permitted, except duplication for research use or educational purposes in electronic or print form. You must obtain permission for any other use. Electronic or print copies may not be offered for sale.

# Combining Rigid Cellulose Nanocrystals and Soft Silk Proteins: Revealing Interactions and Alignment in Shear

Ilona Leppänen,\* Suvi Arola, Alistair W. T. King, Miriam Unger, Hartmut Stadler, Gry Sofie Nissen, Charlotte Zborowski, Tommi Virtanen, Juha Salmela, Harri Setälä, Stephanie Lésage, Monika Österberg, and Tekla Tammelin\*

Natural materials, such as silk and cellulose, have an inspiring set of properties, which have evolved over hundreds of millions of years. In this study, cellulose nanocrystals (CNCs) and regenerated silk fibroin (RSF) are combined to evaluate their suitability for filament formation. This is assessed by tuning and characterizing the interactions between these two materials and finally by studying the alignment of the mixtures under shear. To modify the interactions between CNCs and silk, CNCs with varying surface functionalities (sulfate and/or aminosilane groups) are used. The interactions and compatibility of the two components are investigated using quartz crystal microbalance with dissipation monitoring (QCM-D) and photothermal atomic force microscopy (AFM-IR), which show that ionic interactions induce sufficient binding between the two components. Then, the alignment of the CNC and silk mixtures is evaluated by shear-induced polarized light imaging, which indicates that silk can orientate with the CNCs when not covalently bound. Finally, the potential of the materials for filament formation is tentatively demonstrated using an industrial dry-spinning environment, where CNCs are expected to bring order and alignment, whereas RSF provides soft and more mobile regions to further facilitate the alignment of the final filament structure.

cellulose nanofibrils (CNF) in plants and bacteria and silk nanofibrils in spider and silkworm cocoon silks, are considered to be semicrystalline polymer-like nanofibrils. These are composed of highly ordered nanocrystals that are embedded in a softer amorphous matrix.<sup>[1]</sup> In addition to the material properties, the natural processes by which nature synthesizes these materials have gained a lot of attention. Recent studies have shown that silk is spun from an aquameit, which allows the production of silk under aqueous conditions and ambient temperature with low energy demand.<sup>[2]</sup> This is contrary to the way we are accustomed to processing synthetic polymers, where high temperatures, chemicals, and a lot of energy are needed. In addition, petroleum-based polymeric materials are facing challenges related to environmental concerns, which is why naturally derived materials are gaining more attention. Here, we combine cellulose nanocrystals (CNCs) and silk proteins to evaluate their


applicability to form filaments, which exploit the high tendency of CNCs to align under shear and the softness of the silk proteins, to provide novel material solutions.

Cellulose (C<sub>6</sub>H<sub>10</sub>O<sub>5</sub>)<sub>n</sub> is the primary component of the plant cell walls, where it functions primarily as a structural element. It

## 1. Introduction

In nature, biocomposites consist of both stiff and soft components that are arranged in highly oriented hierarchical structures inducing exceptional mechanical properties. For example,

I. Leppänen, S. Arola, A. W. T. King, T. Virtanen, T. Tammelin  
 Biomaterial processing and products  
 VTT Technical Research Centre of Finland Ltd.  
 Espoo FI-02044, Finland  
 E-mail: ilona.leppanen@vtt.fi; Tekla.tammelin@vtt.fi  
 M. Unger, H. Stadler  
 Bruker Nano Surfaces Division  
 Östliche Rheinbrückenstrasse 49, 76187 Karlsruhe, Germany

 The ORCID identification number(s) for the author(s) of this article can be found under <https://doi.org/10.1002/admi.202300162>

© 2023 The Authors. Advanced Materials Interfaces published by Wiley-VCH GmbH. This is an open access article under the terms of the Creative Commons Attribution License, which permits use, distribution and reproduction in any medium, provided the original work is properly cited.

DOI: 10.1002/admi.202300162

G. S. Nissen, S. Lésage  
 Oxford Biomaterials Ltd. Magdalen Centre  
 Oxford Science Park, Oxford OX4 4GA, UK  
 C. Zborowski, M. Österberg  
 Department of Bioproducts and Biosystems  
 School of Chemical Engineering  
 Aalto University  
 Vuorimiehentie 1, Espoo 02150, Finland  
 J. Salmela, H. Setälä  
 Spinnova PLC  
 Palokärjentie 2–4, Jyväskylä 40320, Finland  
 S. Lésage  
 Oxford Silk Phage Technologies (OSPT)  
 Bioescalator  
 Innovation Building  
 Oxford OX3 7FZ, UK

is composed of repeating  $\beta$ -1,4-linked glucopyranose units resulting in a linear polymer chain.<sup>[3]</sup> These cellulose chains associate with one another, through hydrogen bonding between equatorial hydroxyl groups and hydrophobic stacking of axial non-polar moieties, into a tightly packed semicrystalline structure; forming linear parallel-oriented nanofibrils. Nanofibrils are then bundled into microfibrils, which eventually form wood fibers. Owing to the hierarchical structure of cellulose and semicrystallinity, nanosized components, CNFs, and CNCs can be produced from cellulose fibers by a top-down approach using mechanical,<sup>[4]</sup> chemical<sup>[5]</sup> and enzymatic treatments,<sup>[6]</sup> and combinations of those.<sup>[3]</sup> CNCs extracted from wood are short colloidal particles with lengths ranging from 100 to 200 nm and widths of only a few nanometers (3–5 nm).<sup>[3,7]</sup> They are produced from cellulose nanofibrils by removing the disordered domains using acid hydrolysis leaving the crystalline proportion intact.<sup>[8]</sup> Depending on the acid used, CNCs with different chemical moieties are produced. Sulfuric acid hydrolyzed CNCs carrying negatively charged sulfate groups on the surface are currently commercially available<sup>[9,10]</sup> and are thus also industrially relevant.<sup>[11]</sup> CNCs can also be produced via hydrolysis using hydrochloric acid (HCl)<sup>[12]</sup> and even its vapor,<sup>[13]</sup> however, these result in CNCs, which are practically uncharged with low colloidal stability. Hence, subsequent TEMPO-mediated oxidation can be used to introduce negative charges on the surface.<sup>[14]</sup> CNCs have an abundance of surface hydroxyl groups, which can be easily modified, for example, to increase their compatibility with synthetic polymers to form strong composite materials.<sup>[15,16]</sup> In fact, CNCs have gained a lot of attention due to their outstanding mechanical properties, as previous experiments and analytical models have reported a longitudinal Young's modulus for the crystallites ranging between 56–220 GPa.<sup>[17,18]</sup> Thus, they are widely studied as reinforcing agents in composite materials.<sup>[18]</sup> Aqueous dispersions of CNCs are known to form liquid crystal nematic ordered structures above a certain concentration<sup>[19]</sup> and birefringent gels at even higher concentrations,<sup>[20]</sup> resulting in ordered assemblies when shear is applied.

Silk fibers are produced by silkworms and spiders and the most well-studied natural silk fibers are the domestic silkworm silk (*Bombyx mori*) and the spider dragline silks (*Nephila clavipes* and *Araneus diadematus*). These different silks feature differences in structure and chemical variability in their amino acid sequences.<sup>[1]</sup> *Bombyx mori* silk is commonly used for high-throughput production, for example, in the textile industry to produce silk threads and fabrics since silkworms can easily be cultivated. On the contrary, it is difficult to produce spider silk in large quantities, which is why spider silk proteins are usually manufactured using recombinant DNA techniques, ideally leading to silks that mimic the primary structure of natural spider dragline silk proteins.<sup>[21]</sup> Recombinant spider silk has more high-end applications compared to silkworm silk, for example, in the biomedical field, and can be used to gain fundamental knowledge on the silk assembly mechanism by studying the effect of different protein parts.<sup>[22]</sup> *Bombyx mori* silk is composed of two different proteins, a structural protein fibroin and a coating protein sericin, which holds the fibroin filaments together. The structural protein fibroin is composed of a heavy chain and a light chain linked by a disulfide bond and a glycoprotein. The heavy chain consists of highly repetitive core sequences with both hydrophilic and hydrophobic segments, inducing micelle formation in an aqueous

environment.<sup>[23,24]</sup> The repeating motif, GAGAGS, consisting of glycine, alanine, and serine, is the most dominating part of the core and is the building block for the ordered  $\beta$ -sheet crystallites, which contribute to the high strength of natural silk. The highly oriented crystallites are embedded in an amorphous matrix, which in turn facilitates the high extensibility of the fibers. The combination of these two leads to a material with superb toughness, which outperforms synthetic fibers. Thus, in recent decades it has been of interest to create regenerated silk fibroin (RSF) en route to man-made silk fibers. The common method is to dissolve *Bombyx mori* cocoons in special solvents, which have been found to dissolve silk fibroin and subsequently spin them into fibers using different spinning techniques.<sup>[21]</sup> Researchers have been able to produce regenerated silk fibers with better mechanical properties than their natural counterparts.<sup>[25]</sup>

Nanocellulose has been previously studied as a reinforcing agent with regenerated silk fibroin, to produce various composite materials. For example, electrospun CNC/RSF nanofiber mats,<sup>[26]</sup> CNF/RSF<sup>[27]</sup> and CNC/RSF<sup>[28]</sup> composite films, CNC/RSF composite fibers,<sup>[29]</sup> and RSF hydrogels, reinforced with CNC, bacterial cellulose, or CNF.<sup>[30]</sup> Recombinant spider silk proteins have also been combined with nanocellulose to produce composite fibers,<sup>[31]</sup> and sponge-like materials,<sup>[32]</sup> where interactions between silk and cellulose are enhanced by linking cellulose binding domains to the spider silk proteins. In addition, recombinant spider silk proteins have been functionalized with different affinity domains and motifs to increase the bioactivity of CNF/silk composites.<sup>[33]</sup> All of these studies showed improved mechanical properties with the incorporation of nanocellulose. These studies relied on both physical crosslinking and hydrogen bonding between the two components, while only a few studies combine silk and cellulose by covalent crosslinking.<sup>[34]</sup> Bioconjugation is a common method for cross-linking. This has also been applied to crosslink nanocellulose and proteins, by three different strategies using CNCs with introduced amine, epoxy, and carboxylic acid moieties—commonly used functional groups in bioconjugation.<sup>[35]</sup> Based on the findings by Arola et al.<sup>[35]</sup> N-hydroxysuccinimide-activated ester coupling seems to be the most efficient, however, it is not as specific as the others. “Epoxy amination” is the most specific but the efficiency is rather low. By using “amine-amine” coupling they were able to achieve the best specificity/efficiency ratio. Thus, this was chosen as the most suitable method for this study, to covalently crosslink CNCs and RSF.

In this study, we investigated three different approaches to combine CNCs with RSF to determine the most suitable approach for filament formation. The first two are based on mixing CNCs with varying surface charge with RSF and the third one is based on covalently crosslinking the two components together. We functionalized the CNCs using silanization, a well-established method to modify surfaces that are rich in hydroxyl groups. We aimed to covalently introduce a reactive amine moiety onto the CNC surface, via silanization, using an aminosilane, (3-Aminopropyl)trimethoxysilane (APTMS).<sup>[35–37]</sup> Hereby, we were able to i) modify the surface charge of the CNCs by controlling the degree of surface substitution ( $DS_{\text{surf}}$ ) and ii) use it as a platform for further grafting, that is, covalent “amine-amine” crosslinking between CNCs and RSF. We emphasized detailed characterization of the CNC modifications. For example, to verify the direct attachment of the aminosilanes, we resorted to a

novel liquid-state NMR analysis of nanocelluloses, showing that the functionality is chemisorbed rather than physisorbed. Furthermore, we adopted a method to determine the degree of surface substitution, as only the surface hydroxyl groups are available for modification. After characterization, we combined the functionalized CNCs with RSF and studied the interactions and alignment of these systems. First, we analyzed the interactions between CNCs and RSF by using quartz crystal microbalance with dissipation monitoring (QCM-D). We showed that the unconjugated components adsorbing via electrostatic interactions induce a more favorable attachment of RSF on the CNCs compared to the crosslinked system, as the crosslinking resulted in the formation of spherical nanoparticles of RSF. Further, to visualize the alignment of the materials under shear and to determine their suitability for spinning, we utilized shear-induced polarized light imaging (SIPLI). These results indicated that silk can orientate with the CNCs when not covalently bound. Moreover, the CNCs with the higher negative charge showed the best alignment, in flow, with RSF. Finally, preliminary spinning experiments were conducted for mixtures of amine-CNC+RSF (50/50) and CNC+RSF (50/50), using dry-spinning, which takes inspiration from the way natural fibers are produced. Furthermore, we were able to spin pure amine-CNCs into filaments, which is a noteworthy finding, as only a few studies have shown the successful spinning of pure CNCs.<sup>[38,39]</sup>

## 2. Experimental Section

### 2.1. Materials

Cellulose nanocrystal (CNC) powder was purchased from Cellulose (CelluForce NCV100) (Montreal, Canada). The CNCs were prepared by sulfuric acid hydrolysis with a sulfate content of 246–261 mmol kg<sup>-1</sup>, as reported by the supplier. The width of the crystals was measured using transmission electron microscopy (TEM) (Figure S1, Supporting Information) and the average width was 3.99 nm, which is in the range of the reported values by Cellulose (2.3–4.5 nm). The lengths reported by Cellulose range between 44 and 108 nm. For the CNC surface modification calculations we assume a rhomboid fibrillar crystal cross-section, with a width of 4 nm. Aminosilane, (3-Aminopropyl)trimethoxysilane (APTMS) was purchased from Sigma Aldrich (Finland). Regenerated silk fibroin was provided by Oxford Biomaterials Ltd. (Figure S2, Supporting Information). Succinimidyl-6-hydrazinonicotinate acetone hydrazone (SANH) (bc366de35) was purchased from SYNCEM UG & Co. KG (Felsberg/Altenburg, Germany). Succinimidyl-4-formylbenzoate (SFB) (S0893) was purchased from Tokyo Chemical Industry Co., Ltd. (Tokyo, Japan). QCM-D experiments were performed on AT-cut quartz crystal sensors with a silicon oxide (SiO<sub>2</sub>) surface purchased from Q-Sense AB (Gothenburg, Sweden).

### 2.2. Methods

#### 2.2.1. Silanization of Cellulose Nanocrystals and Determination of Surface Substitution

*Silanization of Cellulose Nanocrystals:* Dried CNC powder was dispersed in either dimethylacetamide (DMAc) or DMAc contain-

**Table 1.** Dispersion parameters for surface silanizations to produce amine-modified cellulose nanocrystals (amine-CNCs).

CNC in DMAc [wt%]	1 wt% LiCl addition	Purification of CNCs	Reactor volume
3	no	no	Radley 250 mL
3	yes	no	Radley 250 mL
3	no	yes	Radley 250 mL
3	yes	yes	Radley 250 mL
1	yes	yes	Radley 250 mL
1	yes	yes	Radley 1000 mL

ing lithium chloride (LiCl) to yield either a 3 wt% or a 1 wt% dispersion; LiCl was used only in small amounts, to swell the CNC structure for it to be more prone to modification.<sup>[40]</sup> To further increase the activity of the surface and determine the effect of surface contamination on the efficiency of the reaction, either non-purified or purified CNCs were used. The purification was performed by Soxhlet extraction for 48 h using ethanol.<sup>[41]</sup> After purification, the CNCs were dried in a vacuum oven (40 °C) and stored in a desiccator. Finally, the sample, 1 wt% purified CNC in DMAc with 1 wt% LiCl, was prepared also in a bigger reactor with more efficient mixing (stirrer paddle (1000 mL) and magnetic stirrer (250 mL)). Silanization was performed using an aminosilane, APTMS, to yield amine functionalized CNCs (amine-CNCs), as described previously also for cellulose nanofibrils and nanocellulose films with slight modifications.<sup>[35,42]</sup> The dispersions presented in **Table 1** were first heated to 80 °C in a Radley reactor (250 mL or 1 L). After the dispersions were hot, the APTMS was added in small portions, within 1 h. 10 mL of APTMS was added per 3 g of CNCs. After all the APTMS was added, the reaction was kept at 80 °C for one more hour. The dispersions were stirred overnight. The 3 wt% samples were purified by quenching with methanol and centrifugation. The samples were first centrifuged (3 min, 10 000 rpm) and the supernatant was discarded. The pellet containing the modified CNC was then dispersed into methanol and centrifuged for 30 min at 10 000 rpm. This step was repeated once. After the last centrifugation, the pellet was dispersed into MilliQ water and dialyzed (MWCO 3.5 kDa) to exchange the residual solvent for water and to remove any remaining reagents. The 1 wt% samples were purified using only dialysis (MWCO 3.5 kDa), as no pellet was formed during centrifugation. This suggested that the CNCs remained as individual nanocrystals and that no significant aggregation had occurred during the modification. Dialysis was performed against distilled water and it was changed twice a day over 4 days. The wt% of these samples decreased quite drastically during the dialysis (from 1 to 0.15 wt%) due to the flow of water inside the dialysis tube. After dialysis, the aqueous amine-CNC dispersions were either freeze-dried or evaporated to the desired wt%, for further analysis. The reaction scheme is presented in **Figure 1**, where APTMS reacts with the surface hydroxyl groups on the CNCs in DMAc with the presence of trace water. Silanization can lead either to physisorbed aminosilane moieties or to the covalent attachment of the aminosilanes (chemisorption), the latter being the preferred form.

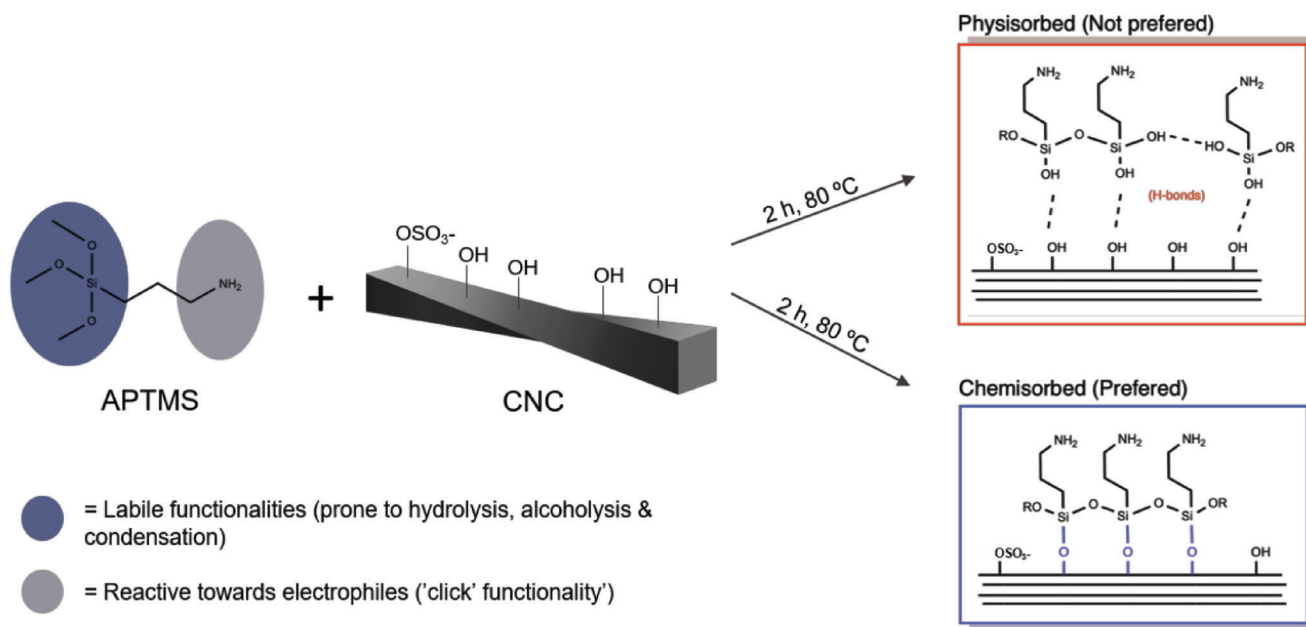


**Figure 1.** Silanization reaction of the cellulose nanocrystals (CNCs) by using an aminosilane, (3-Aminopropyl)trimethoxysilane (APTMS). Silanization can lead either to physisorbed aminosilane moieties or to the covalent attachment of the aminosilanes (chemisorption).

**ATR-FTIR:** Fourier transform infrared spectroscopy measurements (FTIR) were carried out using a Thermo Scientific Nicolet iS50 FT-IR spectrometer with an attenuated total reflectance (ATR) diamond (Thermo Scientific, USA) to identify any changes related to the amination of the CNCs. All spectra were obtained from 32 scans with a resolution of  $4\text{ cm}^{-1}$  throughout the wavenumber range from  $400$  to  $4000\text{ cm}^{-1}$ . Dry films were placed on the ATR crystal and the IR spectrum was measured. At least three repetitions per sample were conducted.

**Elemental Analysis (C, H, N, S):** The carbon (C), hydrogen (H), nitrogen (N), and sulfur (S) content of the samples was measured using a FLASH 2000 series analyzer (Thermo Scientific, USA). Before analysis, the freeze-dried samples were dried in the oven ( $105\text{ }^{\circ}\text{C}$ ) overnight, to remove excess moisture. The elemental compositions of the samples were calculated based on the C, H, and O composition of the anhydroglucose unit (AGU) ( $\text{C}_6\text{H}_{10}\text{O}_6$ ).

**X-Ray Photoelectron Spectroscopy:** X-ray photoelectron spectroscopy (XPS) was used to determine the surface elemental composition and the degree of surface amination of the amine-modified CNCs using a Kratos AXIS Ultra DLD spectrometer with an Al  $K\alpha$  monochromatic X-ray source ( $1486.7\text{ eV}$ ). Survey scans were taken with a  $1.0\text{ eV}$  step and  $80\text{ eV}$  analyzer pass energy, while high-resolution regional spectra were recorded with a  $0.1\text{ eV}$  step and  $20\text{ eV}$  pass energy. During the measurements, the samples were charge-neutralized using slow electrons from a tungsten filament. The base pressure of the system was below  $1 \times 10^{-9}$  Torr. For each sample, XPS measurements were repeated three times on different points of the sample surfaces to check for homogeneity, reliability, and reproducibility of the results. The position of the acquired peaks was charge-corrected relative to the position of the C 1s component for C–C bonding at  $284.8\text{ eV}$ . Analysis of the XPS data was done with CasaXPS software.

**Solid-State  $^{13}\text{C}$  CP-MAS NMR:** Solid-state  $^{13}\text{C}$  cross-polarization (CP) magic angle spinning (MAS) nuclear magnetic resonance (NMR) spectroscopy measurements were carried out to confirm that the amine modification has taken place and to qualitatively assess any crystallinity changes that might occur during silanization. The measurements were performed using an Agilent 600 NMR Spectrometer with a magnetic flux density of  $14.1\text{ T}$ , using a  $1.1\text{ ms}$  contact time and a  $3.0\text{ s}$  delay between a total of  $16\ 000$  successive scans. Power levels for Hartmann–Hahn match were calibrated using  $\alpha$ -glycine, and chemical shifts were calibrated using adamantane by setting the adamantane low field signal to  $38.48\text{ ppm}$ . Spectra were processed using TopSpin 3.6 software.

**Solution-State NMR:** Solution-state NMR was performed on the purified CNCs and amine-CNCs to confirm the covalent attachment of the aminosilane moieties on CNC surfaces. The samples were analyzed using a novel technique, utilizing a partially deuterated ionic liquid-electrolyte solution: tetra-*n*-butylphosphonium acetate:deuterated dimethyl sulfoxide, ( $[\text{P}_{4444}][\text{OAc}]$ ): $\text{DMSO-}d_6$  ( $20:80\text{ wt}\%$ ), mixture.<sup>[43,44]</sup> The samples were dissolved to  $\approx 4\text{ wt}\%$  and analyzed at a probe temperature of  $65\text{ }^{\circ}\text{C}$ . The analysis was performed on a Bruker Avance III 500 NMR spectrometer, equipped with a  $5\text{ mm}$  BBO probe ( $^1\text{H}$ ,  $^2\text{H}$ , BB & Z-grad.  $50\text{ G cm}^{-1}$ ). Multiplicity-edited heteronuclear single quantum coherence spectroscopy (HSQC) experiments were performed in accordance with Koso et al.<sup>[43]</sup> 70% gradient strength was used with a gradient delay of  $300\text{ ms}$  and a gradient pulse length of  $2.5\text{ ms}$ . This allowed for good attenuation of the ionic liquid signals, overlapping the slow-diffusing aliphatic signals. The collected data were processed initially in Topspin 4.1 and then final adjustments and image preparation were completed using Mestrenova 14.



**Determination of the Degree of Surface Substitution ( $DS_{\text{surf}}$ ):** To determine the extent of surface modification, as  $DS_{\text{surf}}$ , it was crucial to understand the cellulose nanocrystal morphology and structure. To provide an in-depth assessment of the degree of surface modification two different cross-sectional models were adopted to calculate the  $DS_{\text{surf}}$  for our CNCs, with either experimentally determined dimensions or theoretical dimensions of a crystallite cross-section. a) The Eyley rhomboid cross-section model,<sup>[45]</sup> with experimentally determined dimensions, 4 nm  $\times$  4 nm ( $L_1 \times L_2$ ), from TEM images, and b) the 18-chain hexagonal model,<sup>[46]</sup> that is, a softwood theoretical model were used. The  $DS_{\text{surf}}$  was calculated according to Equation (1), presented previously by Eyley et al.<sup>[45]</sup> This calculation took into account the number of hydroxyl groups on the surface of the crystals and the two-fold helical twist of the cellulose chain, which resulted in three hydroxyl groups pointing out of the crystal surfaces on every second AGU unit, along the polymers. Thus, only half of the surface hydroxyl, on each (110) or ( $\bar{1}\bar{1}0$ ) plane, were available for modification.

$$DS_{\text{surface}} = \frac{1.5N_{\text{modified}}}{X_{\text{cellulose}}N_{\text{OH}}} \quad (1)$$

where  $N_{\text{modified}}$  is the number of moles of modification (nitrogen or silicon) per gram of product, 1.5 is the number of accessible hydroxyl groups per AGU on the surface,  $N_{\text{OH}}$  is the number of moles of hydroxyl groups per gram on the surface of the CNC,  $X_{\text{cellulose}}$  is the mass fraction of cellulose in the product. Nitrogen (N) content was used as the marker for calculating the degree of surface substitution from the elemental analysis results and Silicon (Si) content was used as the marker to calculate the  $DS_{\text{surf}}$  from the XPS results. The XPS atomic concentrations (at%) were converted to w/w-%, from which  $DS_{\text{surf}}$  can then be calculated, according to Equation (1).

$DS_{\text{surf}}$  can be related to the bulk degree of substitution  $DS_{\text{bulk}}$  using the chain ratio,  $R_c$  presented by Eyley et al., according to Equation (2).<sup>[45]</sup>

$$DS_{\text{bulk}} = R_c \times DS_{\text{surf}} \quad (2)$$

where  $R_c$  is the ratio between the number of cellulose chains on the surface,  $n_{\text{surface}}$ , and the total amount of cellulose chains in the crystal.

**Zeta Potential Measurements:** To evaluate the effect of amination on the stability of the CNCs in aqueous environment zeta potential measurements were performed in water and in varying pH environments (pH 2–10). The measurements were conducted using a particle analyzer instrument (Zetasizer Nano ZS, Malvern, U.K.). The pH values measured at pH 6–8 were measured in 10 mM phosphate buffer used in the QCM-D experiments. For higher (pH 9, 10) and lower (pH 2, 4) pH values, the pH was adjusted using HCl and sodium hydroxide (NaOH), respectively. Furthermore, the zeta potentials of the purified CNCs and amine-CNCs were measured in MilliQ water, which was the environment used for rheology and spinning experiments. Three replicates were measured with concentrations of 0.1–0.01 wt% with three reading each.

## 2.2.2. Bioconjugation and Interactions between Cellulose Nanocrystals and Regenerated Silk Fibroin

**Bioconjugation of Amine-CNCs and RSF by Amine–Amine Coupling:** The crosslinking of RSF to amine-CNCs was performed using a common bioconjugation technique, that is, amine–amine coupling.<sup>[35,47]</sup> The reagents, succinimidyl-6-hydrazinonicotinate acetone hydrazone (SANH) and succinimidyl-4-formylbenzoate (SFB) are heterobifunctional, containing an activated N-hydroxysuccinimide ester (NHS ester) and either a hydrazone or an aldehyde group, respectively. The bioconjugation was performed in three steps: in the first and second steps, the amine-CNCs and RSF were reacted with SANH and SFB, respectively, in separate test tubes. In the third step the modified materials, SANH-CNCs, and SFB-RSF, were crosslinked together either in the QCM-D measurement chamber, to study the crosslinking process, or in lab-scale, to produce a sample for the rheology measurements. For the QCM-D experiments, 20 mL of 1.5 g L<sup>-1</sup> amine-CNC in borate buffer (25 mM, pH 8.9) was reacted with 150  $\mu$ L of 20 g L<sup>-1</sup> SANH dissolved in dimethyl sulfoxide (DMSO) for 3 h at room temperature. For the rheology experiments, 20 mL of 13 g L<sup>-1</sup> amine-CNC in borate buffer (25 mM, pH 8.9) was reacted with 3 mL of 20 g L<sup>-1</sup> SANH dissolved in DMSO for 3 h at room temperature. The amino groups on the amine-CNCs react with the NHS ester moiety yielding the hydrazone reactive species on the amine-CNCs (later referred to as SANH-CNC). The SANH-CNCs were purified by dialysis into MilliQ water (QCM-D) or phosphate buffer (10 mM, pH 7) (rheology) using a molecular weight cutoff of 12000 Daltons. The aldehyde reactive RSF for the QCM-D experiments (later referred to as SFB-RSF) was made by mixing 50 mL of 3 g L<sup>-1</sup> RSF in phosphate buffer (25 mM, pH 7) with 200  $\mu$ L of 20 g L<sup>-1</sup> SFB in DMSO for 3 h at room temperature. For the rheology experiments, 40 mL of 13 g L<sup>-1</sup> RSF in phosphate buffer (10 mM, pH 7) was reacted with 200  $\mu$ L of 20 g L<sup>-1</sup> SFB in DMSO. Lysine residues and the N terminus on the RSF react with the NHS ester moiety on SFB yielding the aldehyde-modified species. The SFB-RSFs, for QCM-D and rheology experiments, were subsequently purified by dialysis to phosphate buffer (10 mM, pH 7). In the third step of the bioconjugation, the two modified components, SANH-amine-CNC and SFB-RSF, were allowed to react in phosphate buffer (10 mM, pH 7) either in the QCM-D measurement chamber or in lab-scale in a glass bottle at room temperature for 6 h crosslinking the materials.

**Quartz Crystal Microbalance with Dissipation Monitoring (QCM-D):** Silica quartz crystals were coated with either purified CNC, amine-CNC, or SANH-CNC thin films by spin coating according to the protocol described by Eronen et al.<sup>[48]</sup> with slight modifications made by Hakalahti et al.<sup>[49]</sup> Briefly, the crystals were rinsed with MilliQ water, dried with nitrogen gas, and placed in an UV-ozonizer (Bioforce Nanosciences, CA) for 10 min to clean the surfaces. Subsequently, an anchoring layer of cationic polymer (polyethylene imine (PEI)) was adsorbed on the crystals by immersing them in an aqueous PEI solution (1 mg mL<sup>-1</sup>). After 30 min the excess PEI was rinsed away by consecutive dipping and rinsing with large amounts of fresh MilliQ water. The different CNC suspensions of 0.15 wt% were sonicated using a Branson 450 Digital Sonifier (400 W tip sonicator, Branson Ultrasonics, Danbury, USA) for 2 min, 25% amplitude. For the

QCM-D experiments, the non-dried amine-CNCs were used. The dispersions were then pipetted onto PEI SiO<sub>2</sub> crystals so that they fully covered the surface of the crystal and then immediately spin-coated (3000 rpm, 1 min) (Model WS-400BZ-6NPP/LITE, Laurell Technologies, North Wales, PA, USA). After spin-coating, the surfaces were rinsed with MilliQ water and dried gently with nitrogen gas followed by heat treatment for 15 min at 80 °C. Interactions between the CNCs (modified and unmodified) and RSF were investigated using the Q-Sense E4 QCM-D instrument (Q-Sense AB, Gothenburg, Sweden). The instrument allows for in situ monitoring of changes in frequency ( $\Delta f$ ) and dissipation ( $\Delta D$ ), as a function of time and at a fundamental resonant frequency (5 MHz), and its overtones. Changes in frequency indicate changes in the adsorbed mass on the crystal and changes in dissipation give information about the viscoelastic properties of the adsorbed layer. The interpretation of the QCM-D data is described in more detail elsewhere.<sup>[50–52]</sup> The adsorption of RSF on purified CNC and amine-CNC surfaces was studied, to establish interactions between the components. In addition, the crosslinking reactions between SANH-CNC and SFB-RSF were monitored by QCM-D. Before the measurements, the crystals coated with different CNCs were stabilized in phosphate buffer (10 mM, pH 7) overnight. RSF and SFB-RSF were diluted in phosphate buffer (10 mM, pH 7) to a concentration of 0.1 g L<sup>-1</sup>. The adsorption of RSF as well as desorption, after rinsing, were monitored as follows: Before the introduction of RSF and SFB-RSF solutions, the coated crystals were stabilized in the QCM-D chambers with phosphate buffer, for  $\approx 1$  h. 0.1 g L<sup>-1</sup> RSF solution was then introduced to the chambers containing the crystals coated with purified CNC and amine-CNC, and 0.1 g L<sup>-1</sup> SFB-RSF solution was introduced to the chamber with the crystal coated with SANH-CNC. The flow rate of the silk solutions was 0.1 mL min<sup>-1</sup> and the adsorption was recorded for  $\approx 1$  h for purified CNC and amine-CNC surfaces, and 6 hours for crosslinking SANH-CNC and SFB-RSF. Subsequently, the surfaces were rinsed with phosphate buffer to identify any desorption of the adsorbed layer. The mass changes on the crystal were monitored by following the changes in frequency and dissipation, as a function of time. Two replicates for each surface were performed.

**Atomic Force Microscopy (AFM):** AFM imaging was used to analyze the surface morphology of the QCM-D crystals coated with different CNCs, before and after adsorption/conjugation of RSF. The characterization was carried out using a NanoTA AFM+ instrument (Anasys Instruments, Bruker, MA, USA) with Mounted Standard Silicon Tapping Mode Probes with Al Reflex coating (Applied Nanostructures Inc., CA, USA). Images of the ultrathin film surfaces were recorded in tapping mode in air, with a scan rate of 0.5 Hz using silicon (Si) cantilevers. The damping ratio was around 0.7–0.85 Hz. For each sample, three different areas were analyzed. The images were not processed by any other means, other than flattening. AFM images were analyzed using Analysis Studio Software 3.15.

**Nanoscale infrared analysis (Photothermal AFM-IR):** Photothermal AFM-IR was performed using a nanoIR3s system (Bruker, MA, USA) with gold-coated Si probes (PR EX nIR2 10, spring constant 0.2 N m<sup>-1</sup>), where the laser source was pulsed at higher eigenmodes of the contact resonance. The samples were analyzed in resonance-enhanced AFM-IR mode with tunable pulse rates using two separate lasers: a 4-chip midIR QCL Laser system and

a Hyperspectral QCL: 780 1950 cm<sup>-1</sup>. Spectra on different locations and IR maps at characteristic wavenumbers (1060 cm<sup>-1</sup> for cellulose and 1630 cm<sup>-1</sup> for silk) were acquired. The AFM-IR images were analyzed using Analysis Studio Software 3.15.

### 2.2.3. Rheology and Alignment of CNC and RSF Dispersions and a Preliminary Spinning Demonstration

**Rheology Measurements and Alignment Under Shear:** Large deformation steady-state rheology measurements were performed using an Anton Paar MCR302 rheometer to reveal the effect of the modification on the dispersions' rheological properties. Dispersions of both purified CNC and amine-CNC at different concentrations (1–4 wt%) were prepared. The dispersions were prepared by dispersing dry CNC powder or freeze-dried amine-CNCs to water and sonicating it at  $\approx 1000$  J g<sup>-1</sup>, which has been shown to be sufficient to break most of the aggregates.<sup>[20]</sup> As the amine CNC dispersions prepared from the freeze-dried material showed some aggregation and flocculation during redispersion, amine-CNC dispersions were also prepared by evaporating the dialyzed amine-CNCs to  $\approx 3$  wt%, from which dilutions were made to 1–3 wt%. The measurements were performed using cone and plate geometry (CP50-1, diameter 49.9614 mm, cone angle 0.984°, gap 0.099 mm) and the shear rate was logarithmically increased from 0.01 to 500–1000 s<sup>-1</sup>. The tests were performed at room temperature. Shear-induced polarized light images (SIPLI) were acquired during the steady-state shear measurements to qualify and visualize the possible alignment and orientation of purified CNCs, amine-CNCs, and their mixtures with RSF. The coupling of optical techniques, with steady-state rheological measurements, gives valuable information about the relationship between macroscopic rheological properties and microscopic structural characteristics of the material. Thus, information on the microstructure, gained by polarized light imaging, gives a better understanding of the rheological behavior of the material. For SIPLI the rheometer was equipped with an optical setup. The method is discussed in more detail elsewhere.<sup>[53,54]</sup> Briefly, the other side of the sheared sample was accessible for visualization, since the rheometer is equipped with a glass plate (P-PTD200+H-PTD200). The optical parts consisted of a color charge-coupled device (CCD) camera, an optical tube that transfers the image telecentrically onto the CCD chip, and an inlet for light. The light source emitted light, which was transferred by the light guide into the optics. This white monochromatic light went through a polarizer to the beam splitter from where it travels to the sample. The sample was thus illuminated with polarized light and the image of this was transferred to the chip of the CCD camera, allowing the recording of changes in the sample structure (alignment, birefringence, crystallization) induced by shear. Cross-polarized light (polarizer oriented perpendicularly to the analyzer) was used in all measurements and an area of 25 mm was directly optically monitored by this setup. The tests were performed at room temperature.

**Dry-Spinning of Silk-CNC Composite Filaments:** Mixtures of purified CNC+RSF and amine-CNC (evaporated)+RSF were spun at 50/50 dry-weight ratios. In addition, amine-CNC (evaporated), purified CNC, and RSF were spun alone, as reference (100%). The solid contents of the spinning dopes were: 7 wt% for

**Table 2.** Elemental analysis results for amine-modified cellulose nanocrystals (amine-CNCs).

Sample	Elemental analysis [wt%]			
	N	C	H	S
CNC (reference)	0	42.72	6.21	0.53
3 wt% CNC <sup>a)</sup>	0.32 ± 0.03	42.00 ± 0.14	6.26 ± 0.06	0.51 ± 0.03
3 wt% CNC + LiCl <sup>b)</sup>	0.35 (0.00)	41.86 ± 0.15	6.26 ± 0.05	0.48 ± 0.04
3 wt% CNC (purified) <sup>c)</sup>	0.33 ± 0.02	40.85 ± 1.28	6.13 ± 0.13	0.49 ± 0.04
3 wt% CNC (purified) + LiCl <sup>d)</sup>	0.37 (0.00)	42.17 ± 0.06	6.19 ± 0.04	0.49 ± 0.03
1 wt% CNC (purified) + LiCl (250 mL reactor) <sup>e)</sup>	0.67 ± 0.04	41.86 ± 0.33	6.17 ± 0.03	0.58 ± 0.01
1 wt% CNC (purified) + LiCl (1000 mL reactor) <sup>f)</sup>	1.13 ± 0.02	41.44 ± 0.25	6.33 ± 0.04	0.57 ± 0.04
	0.95 ± 0.06	38.38 ± 0.02	5.64 ± 0.1	0.38 ± 0.04
	1.04 ± 0.11	38.92 ± 0.9	6.02 ± 0.04	0.37 ± 0.1

<sup>a)</sup> 3 wt% CNC in DMAc (250 mL reactor); <sup>b)</sup> 3 wt% CNC in DMAc + 1 wt% LiCl (250 mL reactor); <sup>c)</sup> 3 wt% CNC (purified) in DMAc (250 mL reactor); <sup>d)</sup> 3 wt% CNC (purified) in DMAc + 1 wt% LiCl (250 mL reactor); <sup>e)</sup> 1 wt% CNC (purified) in DMAc + 1 wt% LiCl (250 mL reactor); <sup>f)</sup> 1 wt% CNC (purified) in DMAc + 1 wt% LiCl (1000 mL reactor).

amine-CNC+RSF, 8wt% for the CNC+RSF, 12 wt% for the silk, and 2 wt% for the amine-CNCs. The spinning experiments were conducted in Spinnova's filament spinning facilities using their R&D spinning device, utilizing a dry-spinning method. Initially, the CNCs (CNCs and amine-CNCs) were mixed separately for 15 min. Next, both CNCs (CNCs and amine-CNCs) and RSF were combined and the mixtures were carefully stirred, with a magnetic stirrer (30 s), to mix them thoroughly. Subsequently, the samples were carefully placed in a 100 mL syringe and fed into a Teledyne pump (Teledyne ISCO, NE, USA), and spun through a nozzle (nozzle diameter = 0.13–0.25 mm) into filaments on a stainless steel substrate with a ceramic surface treatment. The filaments were dried for 10 s under three IR lamps and once they had dried they could be detached from the substrate. Subsequently, the films were placed in a conditioned environment at 25 °C with a relative humidity of 65% overnight. The filaments' mechanical properties, stress, and strain were evaluated using a Tex Techo Instrument (Textechno Herbert Stein GmbH & Co. KG, Mönchengladbach, Germany).

### 3. Results and Discussion

#### 3.1. Attachment of Aminosilanes on CNCs and Determination of the Surface Substitution

##### 3.1.1. Surface Modification and Chemical Characterization of the Amine-CNCs

Surface modification of CNCs was performed using the well-known silanization chemistry, which can lead either to physisorbed aminosilane moieties or to the direct attachment of the aminosilanes (chemisorption), the latter being the preferred form (Figure 1).<sup>[55]</sup> For the modification, we tested different dispersion parameters, presented in Table 1, to find the most suitable conditions to yield maximum amination. The dispersion parameters included the solid content of CNCs (CNC wt% in DMAc), the addition of 1 wt% LiCl, the purification of CNCs before dispersion, and the volume of the reactor. Altogether six different combinations were tested, for which DMAc was chosen as the reaction medium as it is a cellulose compati-

ble solvent, commonly used for cellulose dispersion, dissolution, and modification.<sup>[40,56]</sup> For the chemical characterization of the modified CNCs (amine-CNCs), we used elemental analysis, ATR-FTIR, solid-state NMR, and XPS, which gave evidence that aminosilane functionalities were present in the samples. However, they were not able to show whether the aminosilanes are physisorbed or chemisorbed. Thus, to demonstrate the direct attachment we finally resorted to liquid-state NMR.

First, we performed elemental analysis on the six samples listed in Table 1, to gain preliminary evidence on the success of the chemical modification of the CNCs and the effect of the dispersion parameters. By comparing the amount of nitrogen present in the samples originating from the APTMS molecule, we were able to determine, which of the dispersion conditions led to maximum surface amination. **Table 2** summarizes the elemental analysis results. As expected, elemental analysis results showed no major changes in the C, H, and S content. All samples showed nitrogen, confirming the attachment of the APTMS molecule to our samples. The N content varied between 0.32% and 1.13%. Decreasing the CNC dispersion concentration to 1 wt% led to almost double the amount of nitrogen in the sample, indicating that the reaction is more efficient at more dilute dispersions. Thus, we moved forward with this concentration and prepared the sample in bigger batches (1000 mL reactor). From Table 2, we can observe that the reaction yield could be further increased when up-scaled with only minor deviations between the three batches. The higher degree of modification is most probably due to more efficient mixing in the bigger reactor. In conclusion, we were able to reach maximum amination with the dispersion prepared at low solids content (1 wt%), where the surface was activated by purifying the CNCs accompanied with the 1 wt% LiCl addition. The amination could be further increased by using a bigger reactor with more efficient mixing. Thus, further discussion will focus on the sample, 1 wt% CNC (purified) in DMAc + 1 wt% LiCl.

As a complementary technique for elemental analysis, we applied ATR-FTIR, to detect the amination of the CNC samples (**Figure 2** and **Figure S3**, Supporting Information). As expected, the samples displayed absorption regions, 800–1500 cm<sup>-1</sup> (C–O–C), 3000–3600 cm<sup>-1</sup> (–OH), and 2800–2900 cm<sup>-1</sup> (–CH),



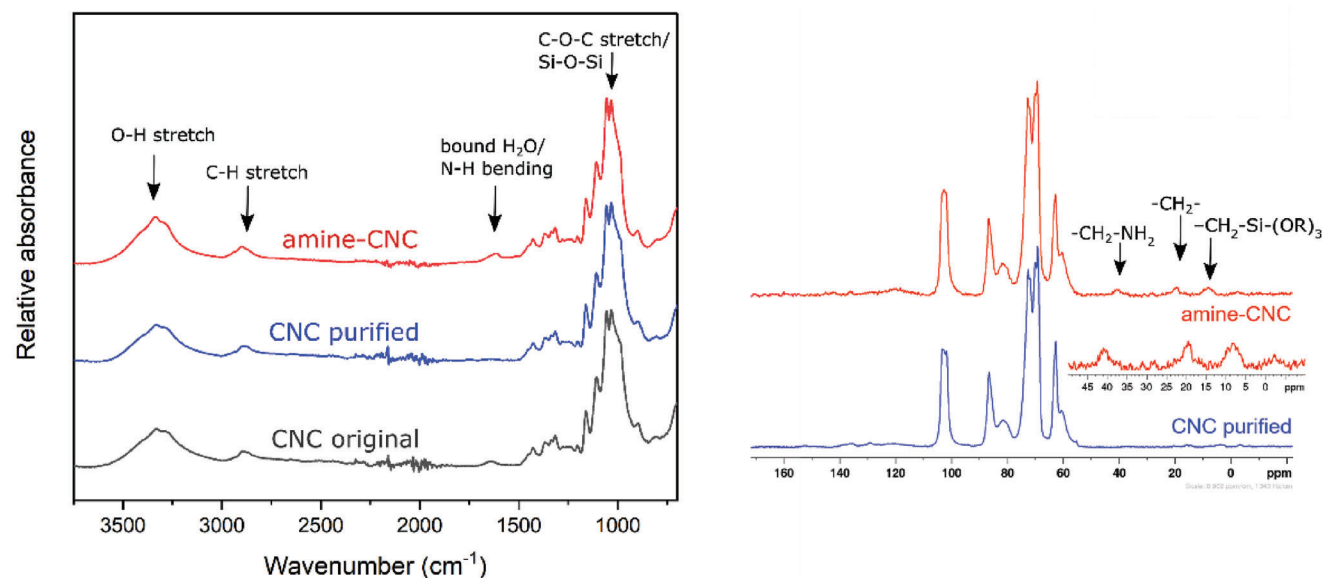


**Figure 2.** Attenuated total reflectance-Fourier transform infrared spectroscopy (ATR-FTIR) (left) and solid-state nuclear magnetic resonance (NMR) (right) spectra of amine-modified cellulose nanocrystals (amine-CNC) (1 wt% CNC (purified) in DMAc + 1 wt% LiCl (250 mL reactor)) and unmodified CNC samples (purified CNC and original CNC) as references. The expansion in the NMR spectra is from the aliphatic region, where the typical peaks for (3-Aminopropyl)trimethoxysilane (APTMS) are located.

typical to that of the cellulose I allomorphs.<sup>[57]</sup> The peak at around  $1640\text{ cm}^{-1}$  may originate from both bound water and N–H bending of the free primary amine present in the APTMS molecule, thus, it is difficult to make any conclusions about the success of the modification. An appearance of a peak around  $1550\text{ cm}^{-1}$ , arising from possible –NH bending, has been reported previously for APTES modifications.<sup>[37,58,59]</sup> However, this peak is not visible in our samples. The absence of this peak does not necessarily indicate an unsuccessful reaction, since the penetration depth of ATR-FTIR is about  $2\text{ }\mu\text{m}$ . Thus, it will record the spectra throughout the CNCs and not only from the CNC surface, where the modification has taken place. The typical peaks for Si–O–Si and Si–O–C are overlapping with the strong C–O–C band and thus it is difficult to differentiate these based on the ATR-FTIR.<sup>[37,58]</sup> However, slight differences in the shape of the fingerprint area can be distinguished between the unmodified and modified CNC samples, giving some indication of success.

Next, we performed solid-state  $^{13}\text{C}$  CP/MAS NMR (Figure 2) on our samples. The presence of signals corresponding to the expected ppm values for aliphatic signals from APTMS are present in the amine-CNC sample, but not in the unmodified CNC sample. Three new weak signals in the amine-CNC spectrum are observed between 10 and 50 ppm, which correspond to  $-\text{CH}_2-\text{NH}_2$  (around 40 ppm),  $-\text{CH}_2-$  (around 20 ppm), and  $-\text{CH}_2-\text{Si}-(\text{OR})_3$  (10 ppm), of the aminopropyl groups of the APTMS reagent. Similar observations have been reported also previously.<sup>[37,42,60]</sup> In addition, the spectra did not show any changes in the cellulose I form, as characterized by no visible changes in the broad and sharp signals for the C4 region. Furthermore, the effect of DMAc/1 wt% LiCl on the crystallinity of the CNCs was also evaluated from the solid-state NMR data by peak fitting and there was no major change in crystallinity, 44% and 52% for amine-CNCs and purified CNCs in water, respectively. This showed that the addition of 1 wt% LiCl as an activating agent was not too high

to start dissolving the cellulose or causing significant changes in the crystalline form.

To gain information on the elemental composition on the outermost surface of the CNCs, we used a surface-sensitive technique, XPS. Amination was confirmed by the appearance of additional core-level peaks in the XPS survey spectra, attributed to nitrogen (N 1s) around 400 eV and to silicon (Si 2p and Si 2s) around 102 and 150 eV, in addition to the C and O and S peaks, which were visible also for the reference materials (Figure S4, Supporting Information). The elemental compositions (at%) of C, O, N, S, and Si of the samples are presented in Table 3 and Table S1, Supporting Information. We observed a ratio between the Si and N content of around 1.1 (Table 3, Table S1, Supporting Information) for our amine-CNC samples, which is close to the theoretical ratio expected from the structure of the APTMS molecule.

The high-resolution N 1s spectra (Figure 3) can be deconvoluted into two areas, corresponding to two different types of nitrogen bonds in the sample ( $\text{NH}_2$  and  $\text{NH}_3^+$ ), revealing the presence of charged amine groups on the surface. In addition, the high-resolution C 1s spectra (Figure 3) can be deconvoluted into different areas, giving information on how the carbons are bonded. These four bonds correspond to C–O/C–N at 286.5 eV, C–C at 284.8, O–C–O at 288.0 eV, and O–C=O at 289.1. The relative abundance of these carbon bonds (at%) is presented in Table 3. Theoretically, the cellulose molecule itself, without any modifications, does not contain the C–C component, that is, carbons without oxygen neighbors. However, this band is always detected even for pure cellulose samples. It has been shown to arise from impurities and remnants of lignin, and hemicellulose, on the cellulose surfaces.<sup>[61,62]</sup> In addition, impurities, such as aromatics and aliphatics, have been shown to accumulate on CNC surfaces, leading to a reduction in the reactivity.<sup>[41,63]</sup> The abundance of C–C bonds for the CNC powder was 14.8%, which is relatively high for unmodified cellulose. The atomic

**Table 3.** X-ray photoelectron spectroscopy (XPS) results showing the elemental composition (at%) and relative abundance of carbon species (at%), of amine-modified cellulose nanocrystals (amine-CNCs) (1 wt% CNC (purified) in DMAc + 1 wt% LiCl (1000 mL reactor)), and reference cellulose nanocrystals (CNC powder and Soxhlet purified CNC powder).

Sample	Elemental concentration [at%]					Relative abundance of carbon bonds [at%]			
	C	O	N	S	Si	C–C	C–O/C–N	O–C–O	O–C=O
CNC powder (Ref.)	61.7	37.2	0	0.5	0.2	14.8	66.3	16.4	2.5
Soxhlet purified CNC powder (Ref.)	58	40.8	0	0.7	0	4.4	74.8	18.7	2.1
amine-CNCs	57.8	40.5	0.8	0.7	1.0	7.8	73.3	17.5	1.4

percentage of C–C bonds is decreased to 4.4% by Soxhlet extraction, indicating the extraction efficiently removed impurities making the surface more prone to modification. An increase in the relative abundance (at%) of C–C bonds originating from the APTMS molecule, was observed as expected.

While all the results gained so far from elemental analysis, ATR-FTIR, solid-state NMR, and XPS show that the APTMS species are present in the samples, they do not confirm the direct attachment of the aminosilanes on the CNCs, that is, whether they are physisorbed or chemisorbed.

### 3.1.2. Evidence Supporting Covalent Attachment

Finally, we resorted to solution-state NMR to show that the functional group is covalently attached, that is, chemisorbed. We employed diffusion-edited  $^1\text{H}$  NMR on the amine-CNC sample, 1 wt% CNC (purified) in DMAc + 1 wt% LiCl (1000 mL reactor) (Figure 4). This technique allows for editing out the slow-diffusing species, that is, it would have the effect of attenuating the physisorbed material but keeping the chemisorbed signals in the spectrum. Proof of chemisorption versus physisorption is a long-standing question for the silanization platform.<sup>[64]</sup> Due to the potential for the introduction of a wide range of novel reactive or “click” functionalities, confirming covalent attachment is critical for the reduction of downstream leaching of the introduced functionalities, from the surface of celluloses.

The amine-CNC spectrum was compared to the normalized  $^1\text{H}$  spectrum for the unmodified CNCs (Figure 4a) and the diffusion-edited  $^1\text{H}$  spectrum for the unmodified CNCs (Figure 4b). The effect of diffusion editing can be clearly observed when comparing the two spectra of the unmodified CNCs. In

Figure 4b, the ionic liquid signals are almost completely attenuated, after applying diffusion editing. In Figure 4c, it can be observed that there are clear alkyl resonances corresponding to the APTMS-like moieties, retained after applying the diffusion editing. When compared to APTMS in the  $[\text{P}_{4444}][\text{OAc}]:\text{DMSO-}d_6$  electrolyte (Figure 4d), there is a clear overlap observed. This indicates that by using this silanization procedure, the reagent has become chemisorbed. In addition to this evidence, we also suspended the amine-CNCs in  $\text{DMSO-}d_6$  to see if there was any physisorbed material that could be extracted from the surface (Figure 4e). In fact, no resonances corresponding to APTMS can be observed, however, traces of DMAc were observed, retained in the sample after the silanization procedure (including after dialysis). These two methods give strong support for covalent attachment, that is, chemisorption. Where possible ambiguity would arise would be from the interpretation of the diffusion-edited  $^1\text{H}$  experiment results, as it does not demonstrate a coupling-dependent correlation between species but rather shows that both the cellulosic and silyl species are both diffusing at a very slow rate, compared to the low molecular weight species. However, as we do not observe the extraction of any silyl species into  $\text{DMSO-}d_6$  (Figure 4e), the silyl species seems to be strongly bound to the CNCs, at least under these solvent conditions. In the future, diffusion-editing could be used to assess the connectivity between different species using different solvents, which are relevant for processing the materials.

### 3.1.3. Calculation of Degree of Surface Substitution

The CNCs used in this study are derived from plants having a majority of the  $\text{I}_\beta$  crystalline allomorph structure. The early

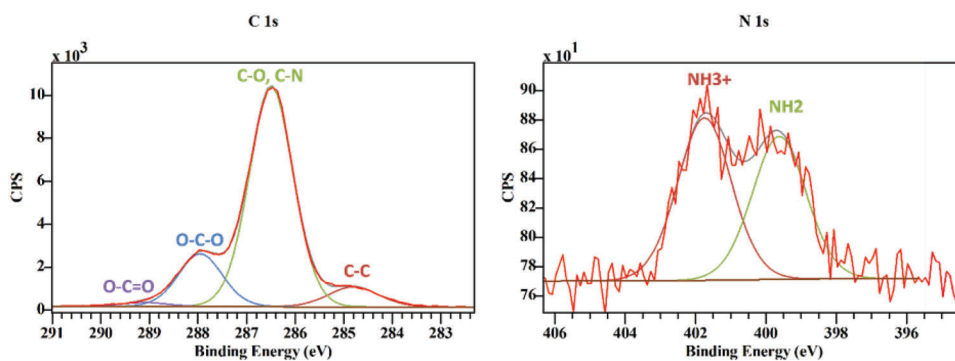


**Figure 3.** High-resolution X-ray photoelectron spectroscopy (XPS) spectra of C 1s and N 1s for amine-modified cellulose nanocrystals (amine-CNCs), 1 wt% CNC (purified) in DMAc + 1 wt% LiCl (1000 mL reactor).

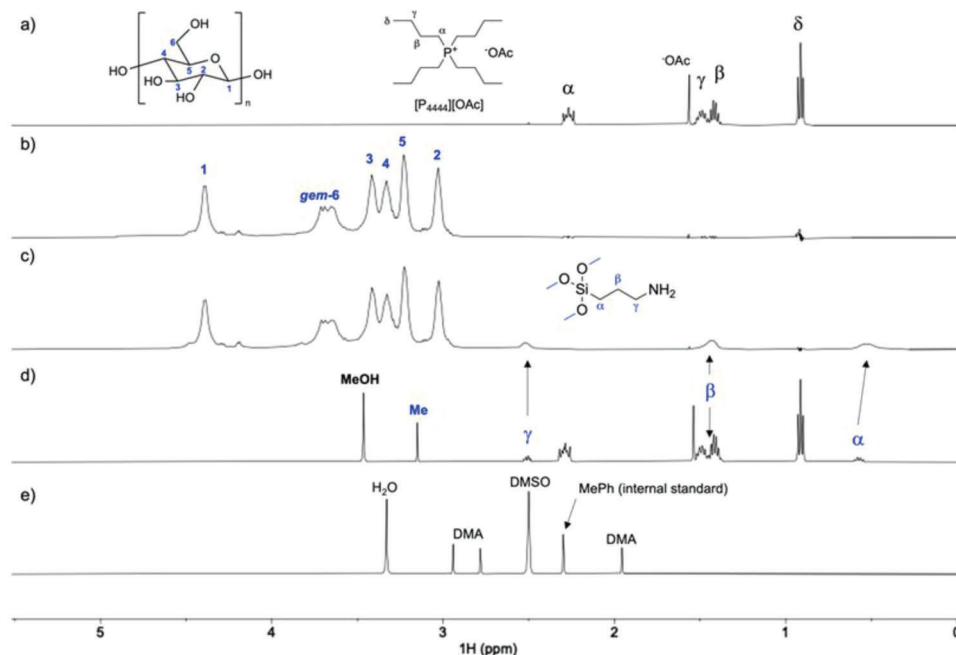


**Figure 4.**  $^1\text{H}$  spectra: a)  $^1\text{H}$  spectrum of unmodified cellulose nanocrystals (CNCs) in  $[\text{P}_{4444}][\text{OAc}]:\text{DMSO}-d_6$ , b) diffusion-edited  $^1\text{H}$  spectrum of unmodified CNCs in  $[\text{P}_{4444}][\text{OAc}]:\text{DMSO}-d_6$ , c) diffusion-edited  $^1\text{H}$  spectrum of amine-CNCs in  $[\text{P}_{4444}][\text{OAc}]:\text{DMSO}-d_6$ , d)  $^1\text{H}$  spectrum of (3-Aminopropyl)trimethoxysilane (APTMS) in  $\text{DMSO}-d_6$ , e)  $^1\text{H}$  spectrum of  $\text{DMSO}-d_6$ -extracted amine-CNCs (with toluene as internal standard).

fibrillar model cross-sections for the  $I_\beta$  crystalline structure were thought to consist of 36 cellulose chains based on the composition of the cellulose synthase complexes (CSCs).<sup>[65]</sup> These models are commonly presented as having a square cross-section with only (110) and (1 $\bar{1}$ 0) planes on the surface, as suggested by solid-state NMR data.<sup>[66,67]</sup> However, currently the 36-chain model has been displaced by the 24-chain and 18-chain models, which favor the formation of more hexagonal shapes having faces made up of the (110), (1 $\bar{1}$ 0), and (200) Miller index planes.<sup>[46,68–71]</sup> Based on the literature, the 18-chain model for softwood with a 234432 arrangement of chains is currently the most favored.<sup>[68–70,72]</sup> Moreover, the only model in the literature to calculate  $\text{DS}_{\text{surf}}$  from experimentally determined crystallite sizes is the calculation method described by Eyley et al.<sup>[45]</sup> This is for an early square (rhomboid) model, with only the (110) and (1 $\bar{1}$ 0) planes at the surface, that is, all surfaces contain OH groups due to the absence of the (200) plane.<sup>[73]</sup> For our calculations, we have adopted the 18-chain hexagonal model (234432) and the rhomboid model presented by Eyley et al., but recognize there are variations depending on the species and processing history.<sup>[72]</sup> Furthermore, the true shape of CNCs is shown to be irregular consisting of aggregated structures of a few crystallites even after sonication.<sup>[74]</sup> Thus, the Eyley rhomboid model based on experimentally determined dimensions presents a good alternative to calculate the available hydroxyl groups for modification. In conclusion, for our CNCs, we adopted the 18-chain hexagonal (234432) and the Eyley rhomboid cross-section with dimensions 4 nm  $\times$  4 nm ( $L_1 \times L_2$ ), which have been determined from TEM images.

We used elemental analysis and XPS data to calculate the degree of surface substitution ( $\text{DS}_{\text{surf}}$ ), using Equation (1), for the amine-CNCs based on the measured average nitrogen (N) and silicon (Si) content, respectively. The calculated  $\text{DS}_{\text{surf}}$  values are

converted to  $\text{DS}_{\text{bulk}}$  by Equation (2). In addition, we utilized the liquid NMR data to give an accurate  $\text{DS}_{\text{bulk}}$  corroboration for the aminated CNCs. The  $\text{DS}_{\text{surf}}$  and  $\text{DS}_{\text{bulk}}$  values are presented in **Table 4**. The degree of substitution was determined for two different CNC models a) the Eyley rhomboid model, with experimentally determined dimensions, and b) the 18-chain hexagonal model, that is, a softwood theoretical model. Example calculations for the DS data are provided in the Supplementary information. Interestingly, the values for the degrees of substitution are very similar between the two models, experimental and theoretical, and the calculated  $\text{DS}_{\text{bulk}}$  values from XPS and elemental analysis data are close to the  $\text{DS}_{\text{bulk}}$  derived from the NMR data.

The theoretical maximum degree of surface substitution ( $\text{DS}_{\text{max}}$ ) for the CNCs is 1.5, however, as suggested by Eyley et al. it is unlikely it will be  $> 1$  due to the relative unreactivity of the hydroxyl group at  $\text{C}_3$  as it is taking part in the intramolecular hydrogen bonding. Thus the % of maximum is calculated by comparing the  $\text{DS}_{\text{surf}}$  to  $\text{DS}_{\text{max}} = 1$ . It should be noted that the CNCs used are sulfated, which means a small fraction of the available hydroxyl groups for modification have already been modified. This corresponds to approximately every eight primary hydroxyl replaced by a sulfate group.

## 3.2. Adsorption and Bioconjugation Studies between CNCs and RSF

### 3.2.1. QCM-D Measurements to Study the Physical Adsorption of RSF on the CNC Surfaces

Interactions occurring between CNCs and RSF in mixtures of purified CNC + RSF and amine-CNC + RSF, were revealed using

**Table 4.** Degree of surface ( $DS_{\text{surf}}$ ) and bulk ( $DS_{\text{bulk}}$ ) substitution for amine-modified cellulose nanocrystal (amine-CNC sample), 1 wt% CNC (purified) in DMAc + 1 wt% LiCl (1000 mL reactor) determined from elemental analysis, X-ray photoelectron spectroscopy (XPS), and solution-state nuclear magnetic resonance (NMR) results.

Method	Experimental <sup>a)</sup>			Theoretical <sup>b)</sup>		
	$DS_{\text{surf}}$	$DS_{\text{bulk}}$	% of maximum <sup>c)</sup>	$DS_{\text{surf}}$	$DS_{\text{bulk}}$	% of maximum <sup>c)</sup>
Elemental analysis (N, wt%)	0.24	0.13	24	0.20	0.13	20
XPS (Si, at%)	0.23	0.13	23	0.19	0.13	19
NMR (integrated peak area) <sup>d)</sup>	-	0.070	12	-	0.070	11

<sup>a)</sup> Experimental values are calculated based on Eyley rhomboid model, with experimentally acquired crystal dimensions (rhomboid,  $4 \times 4$  nm); <sup>b)</sup> Theoretical values are calculated based on the 18-chain hexagonal model, i.e., a softwood theoretical model; <sup>c)</sup> % of maximum is calculated by comparing the  $DS_{\text{surf}}$  to the maximum degree of surface substitution ( $DS_{\text{max}} = 1$ ); <sup>d)</sup>  $DS_{\text{bulk}}$  gained from the NMR by integrating the peak area (Equation (S1), Supporting Information).

quartz crystal microbalance with dissipation monitoring (QCM-D). This method is highly surface sensitive and gives information on whether ionic interactions induced simply by mixing the two components together are enough for sufficient binding or whether covalent crosslinking via bioconjugation is needed. Cellulose is not very prone to non-specific protein adsorption, which originates from its hydrophilic nature, which is why nanocellulose has been used as an antifouling coating for membrane applications.<sup>[75,76]</sup> Thus, electrostatic or covalent crosslinking is usually needed for fully irreversible adsorption. First, we monitored the adsorption of RSF on purified CNC and amine-CNC surfaces in situ (Figure 5a,b). After introducing RSF on the purified CNC surface, there was a clear decrease in the frequency indicating that RSF adsorbed (Figure 5a). Once the system had stabilized, the system was rinsed using phosphate buffer, which caused a positive change in frequency indicating that some RSF is desorbed from the surface. The overall change was still negative indicating that a thin layer remains adsorbed on the surface. It can be expected that the excess amount of RSF, which is not directly interacting with the CNC layer was desorbed and only a thin monolayer of RSF remained on the CNC surface. A similar phenomenon could be observed for the adsorption of RSF onto an amine-CNC surface (Figure 5b), which has both positive and negative surface charges, originating from the amine groups and sulfate groups respectively. RSF was adsorbed but rinsing detached the excess amount of RSF from the surface. Comparing these two systems, the adsorption phenomena are slightly different as less protein was desorbed from the amine-CNC surface with rinsing compared to the purified CNC surface. However, the overall decrease in frequency after  $\approx 60$  min of rinsing is slightly higher for the purified CNC surface ( $-18$  Hz) compared to the amine-CNC surface ( $-14$  Hz) and thus more protein was adsorbed on the purified CNC surface at the end of the experiment. These results indicate that the interactions induced by physical adsorption are sufficient to induce binding between amine-CNCs/CNCs and RSF and that amination of the CNCs is not necessarily needed. However, as the amine-CNCs bear also positively charged surface groups, this could facilitate stronger attraction of RSF onto the amine-CNC surface, which could explain the lower amount of desorbed RSF with rinsing. Silk fibroin has an estimated theoretical isoelectric point (pI) of around 4.5, meaning that above this pH RSF is negatively charged. However, because of the strong acidic sulfate groups, the amine-CNCs are negatively charged at a wide pH range and the difference between the overall adsorption is not that significant since both systems

are still anionic,  $-27$  and  $-33$  mV for amine-CNCs and purified CNCs, respectively, at our measurement conditions (10 mM phosphate buffer, pH 7) (Figure S5, Supporting Information).

AFM images of the QCM-D crystals before and after adsorption on purified CNC (Figure 5c) and amine-CNC (Figure 5d) are presented beneath the frequency and dissipation curves. For purified CNC and amine-CNC, very little difference can be observed on the surface after the adsorption (Figure 5c,d right). The height profiles have smoothed to some extent after adsorption, however, a single protein is difficult to see on the conventional AFM. The adsorption of the proteins was confirmed by photothermal AFM-IR, which gives information on the chemical composition of the surfaces. The AFM-IR images (Figure 5e,f, right column) showed typical adsorption peaks for proteins at  $1630 \text{ cm}^{-1}$  confirming that the proteins had adsorbed on top of the CNCs forming a thin monolayer. The images on the left-hand side are before adsorption and the images on the right, are after adsorption. Before adsorption, the photothermal AFM-IR map shows the areas in yellow/red where the  $1060 \text{ cm}^{-1}$  wavenumber, typical for cellulose, is visible. After adsorption, the surface is treated with wavenumber  $1630 \text{ cm}^{-1}$ , which is typical for proteins. The areas rich in this wavenumber are shown in yellow/red. In addition, the spectra collected from different positions show the typical carbonyl-based vibrations for proteins, around  $1630 \text{ cm}^{-1}$  (Figure S6, Supporting Information). This correlates with the ATR-FTIR spectra for pure RSF and the two CNCs (Figure S6, Supporting Information).

### 3.2.2. Bioconjugation of CNCs and RSF in QCM-D

Next, we assessed whether we could maximize the binding between RSF and CNCs by crosslinking the two materials by well-known bioconjugation chemistry using amine-amine coupling (SANH-CNC + SFB-RSF).<sup>[35,47]</sup> This system is very different from the physical adsorption discussed in Section 2.2.1 as the binding discussed here is guided by a chemical reaction rather than by spontaneous adsorption driven by entropic changes. Comparing Figure 5a,b, and 6a we can observe that the kinetics for the crosslinking reaction between SANH-CNCs and SFB-RSF (Figure 6a) differed greatly from the kinetics induced by only physical interactions between CNCs and RSF (Figure 5a,b), as the crosslinking reaction proceeded slower compared to the physical adsorption. In addition, a larger negative change in frequency,  $\approx -225$  Hz, was detected for the crosslinking reaction at the end



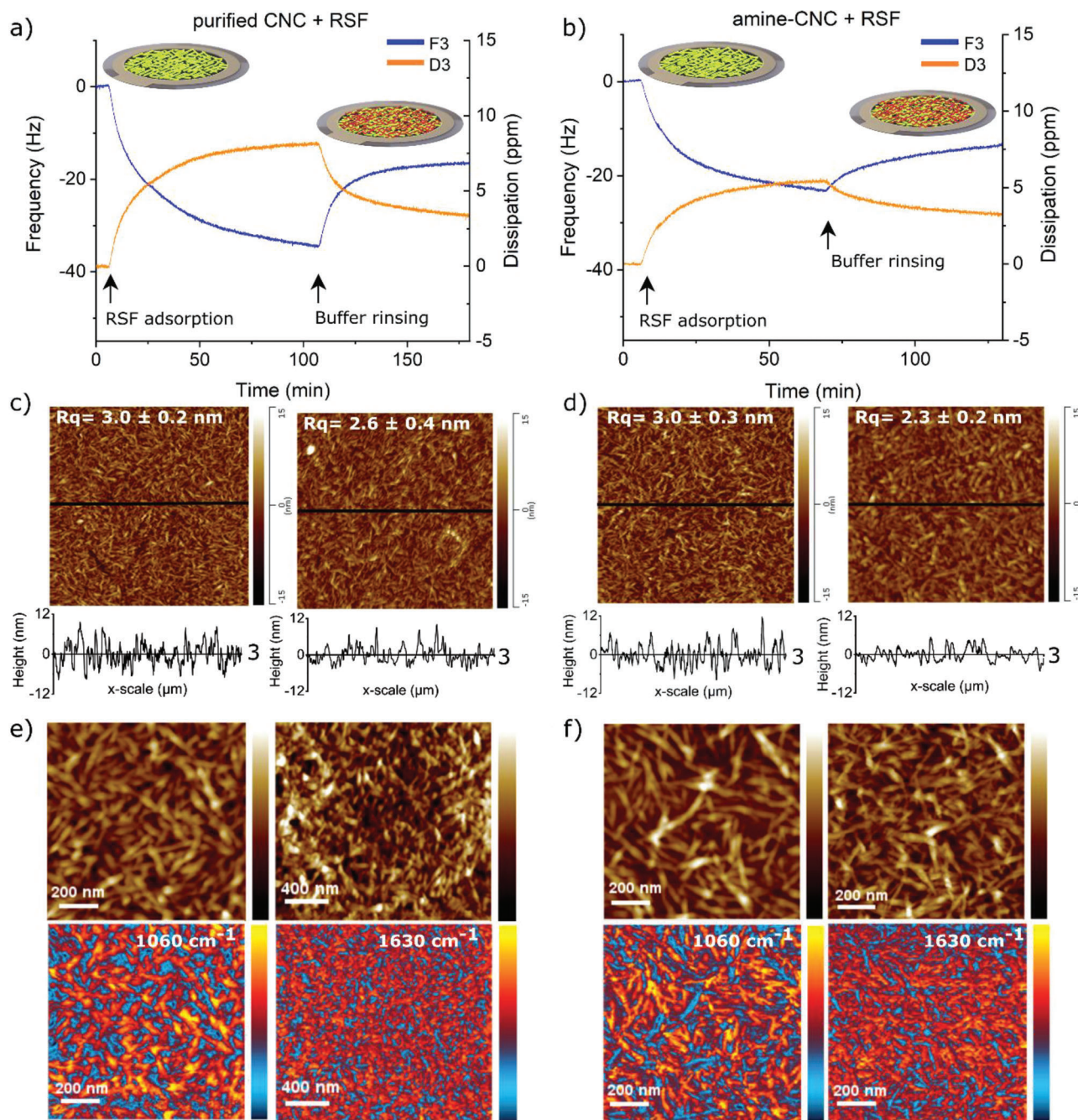


**Figure 5.** Quartz crystal microbalance with dissipation monitoring (QCM-D) frequency and dissipation graphs showing adsorption of regenerated silk fibroin (RSF) onto a) the purified cellulose nanocrystal (CNC) surface, and b) the amine-CNC surface. Atomic force microscopy (AFM) images of the QCM-D surfaces for c) the purified CNCs, and d) the amine-CNCs, before (left) and after (right) RSF adsorption. c,d) Roughness values ( $R_q$ ) presented for the AFM images both before and after adsorption of RSF. Photothermal AFM-IR images of the QCM-D crystals coated with e) purified CNC and f) amine-CNC before (left) and after (right) RSF adsorption. In the upper panel, AFM topographical images, and in the lower panel the corresponding photothermal AFM-IR images, of the QCM-D crystals, collected at  $1060\text{ cm}^{-1}$  (before RSF adsorption) and  $1630\text{ cm}^{-1}$  (after RSF adsorption). The height scale for (e) and (f) is 20 nm. The yellow/red color indicates where the signal for the measured wavelength is the most intense and the blue areas where it is less intense.

of the experiment, compared to physical adsorptions, which stabilized around  $-18$  and  $-14$  Hz for CNCs and amine-CNCs, respectively, after 1 h of rinsing. No desorption induced by rinsing was detected for the crosslinked system indicating irreversible amine-amine coupling. The crosslinking reaction did not stabi-

lize to a certain level but rather increases over time. This may be because SFB-RSF is adsorbed in a specific conformation, due to the restriction of the crosslinking chemistry. Thus, there is more room for more proteins to adsorb. It is also possible that SFB-RSF starts coupling with the free primary amine groups on the already

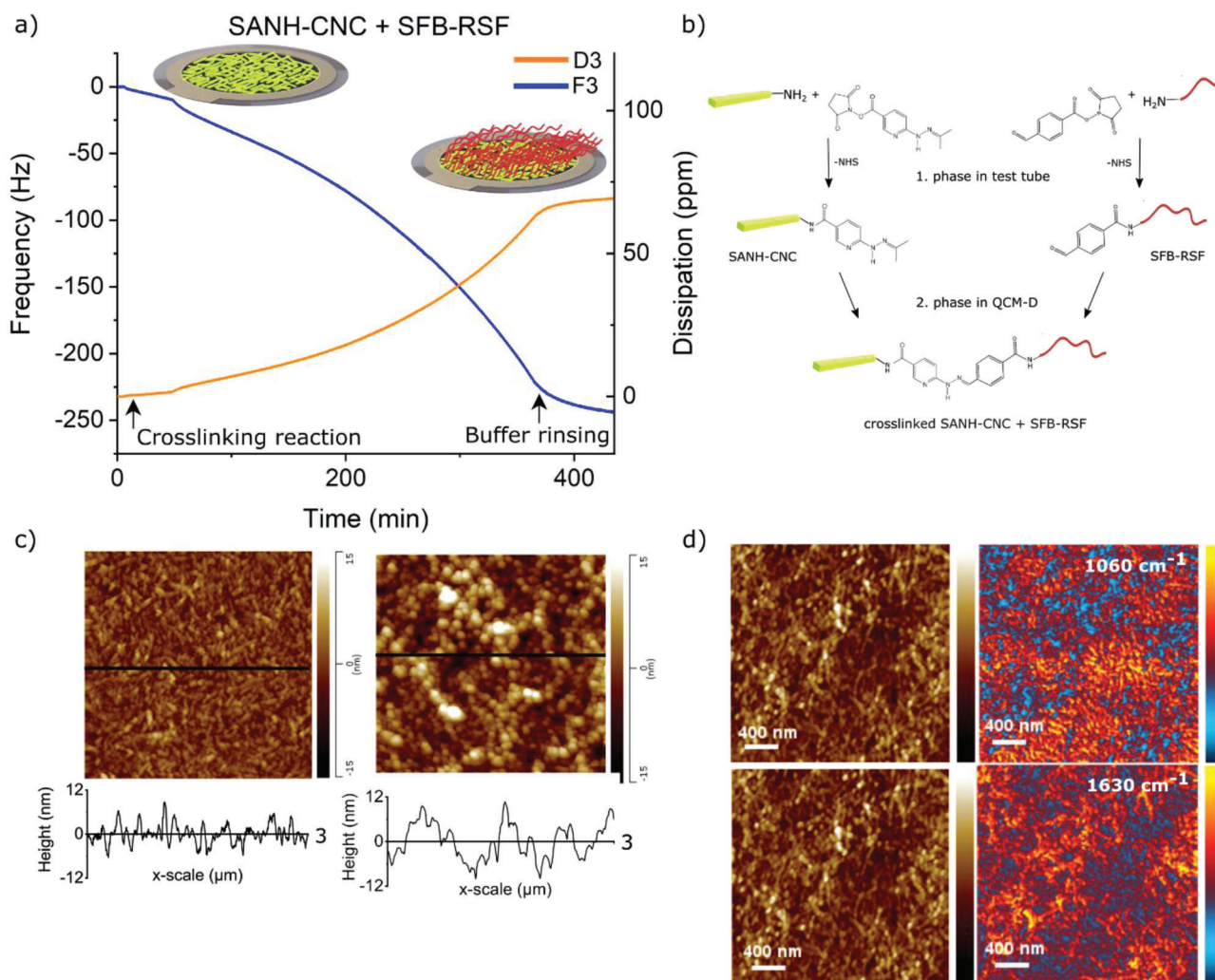


**Figure 6.** a) Quartz crystal microbalance with dissipation monitoring (QCM-D) frequency and dissipation graphs showing the crosslinking reaction between succinimidyl-6-hydrazinonicotinate acetone hydrazone modified cellulose nanocrystals (SANH-CNCs) and succinimidyl-4-formylbenzoate modified regenerated silk fibroin (SFB-RSF) occurring in QCM-D. b) Crosslinking scheme. 1) phase: amine-CNCs and RSF are modified separately in test tubes with heterobifunctional reagents, SANH, and SFB, respectively to yield SANH-CNC and SFB-RSF. 2) phase: the crosslinking reaction between SANH-CNC and SFB-RSF was performed in QCM-D, where SANH-CNCs, carrying a labile (acetone) protected hydrazine moiety, react with the aldehyde group on the SFB attached to RSF, forming a stable hydrazone linkage. The time for this crosslinking reaction (SANH-CNC + SFB-RSF) takes  $\approx 6$  h to proceed and, thus, the QCM-D experiment for the crosslinking was run for a longer time than the physical adsorption experiments. c) Atomic force microscopy (AFM) images of the QCM-D crystal surface before (left) and after (right) the measurement. d) AFM height images of the QCM-D crystals after crosslinking and their corresponding photothermal AFM-IR images at  $1060\text{ cm}^{-1}$  (top row) and  $1630\text{ cm}^{-1}$  (lower row).

attached SFB-RSF, as necessarily not all of the amine groups on RSF have been modified with SFB. However, this Schiff base formation between primary amines and aldehydes is a relatively labile functionality under aqueous conditions. Thus, the linkage may not be stable enough to form a permanent link. This could, however, explain the thicker layer that is formed. Additionally, the change in dissipation is higher for the crosslinking reaction indicating that a greater amount of water was also adsorbed with the proteins.

For the crosslinking layer, shown in Figure 6c, a clear difference can be observed in the AFM images of the surface after the measurement (right), indicating a high amount of RSF is attached. In addition, the protein is not adsorbed as a monolayer

but rather as spherical nanostructures. The photothermal AFM-IR maps (Figure 6d) are both after adsorption and clearly show the areas, which contain more cellulose ( $1060\text{ cm}^{-1}$ , yellow/red areas), and areas where the protein carbonyls at  $1630\text{ cm}^{-1}$  are stronger (yellow/red areas). In addition, the photothermal AFM-IR spectra collected at various positions on the surface correlate well with the ATR-FTIR spectra of the crosslinked system (Figure S7, Supporting Information). In conclusion, the binding between CNCs and RSF could be increased by crosslinking the components by amine-amine-coupling. However, this strong binding induced the formation of spherical protein nanostructures on the CNC surface, which may affect the ability of the CNC crystallites and the protein to orientate under shear.



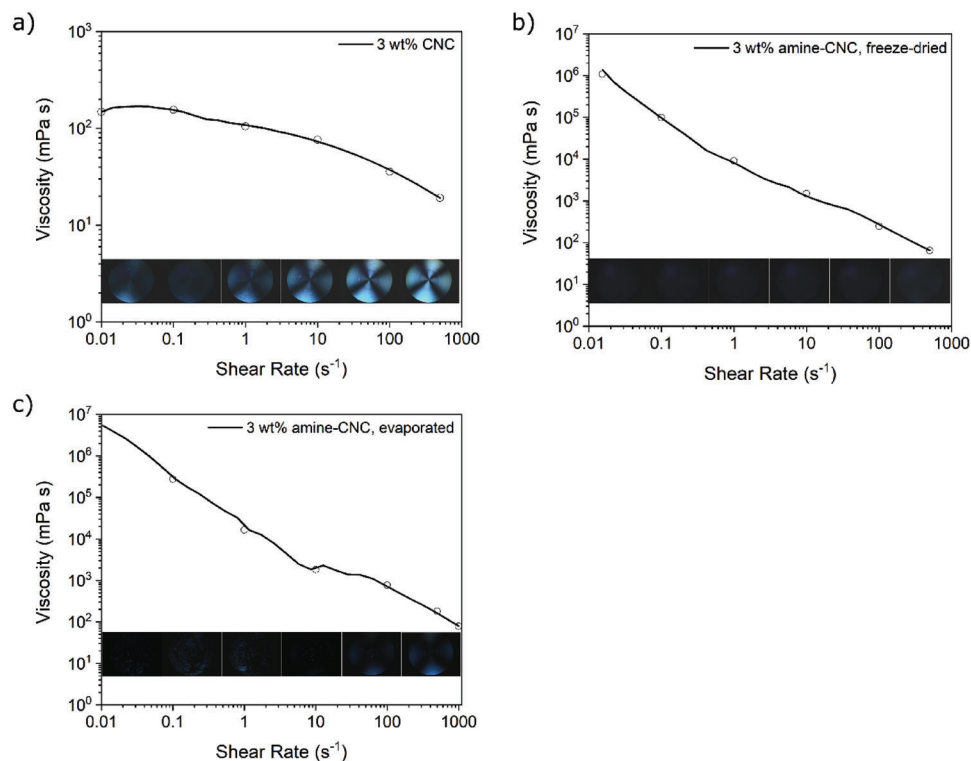


**Figure 7.** Steady-state shear viscosity curves and shear-induced polarized light images (SIPLI) as insets for a) purified 3 wt% cellulose nanocrystal (CNC) dispersion, b) 3 wt% amine-CNC dispersion prepared from freeze-dried material, and c) 3 wt% amine-CNC dispersion, evaporated to 3 wt% from dialyzed material.

### 3.3. Rheology and Alignment of CNC and RSF Dispersions and a Preliminary Spinning Demonstration

#### 3.3.1. Rheological Properties and Alignment of CNCs and RSF

First, we studied the large deformation steady-state rheology of both purified CNCs and amine-CNCs to reveal the effect of the modification on the dispersions' rheological properties. **Figure 7** shows the viscosity curves for 3 wt% purified CNC (Figure 7a) and 3 wt% amine-CNC dispersions (Figure 7b,c). Viscosity curves for the other wt% dispersions are reported in Figure S8, Supporting Information. The purified CNC sample shows typical rheological behavior for lyotropic liquid crystals, as reported previously.<sup>[77]</sup> Three distinct regions can be identified for samples 2–4 wt% (Figure 7 and Figure S8, Supporting Information), which are 1) shear-thinning due to alignment of liquid crystal domains, 2) plateau region, where all domains have been aligned along the shear and 3) a second shear-thinning region, where the domains are destroyed, and individual rods align. Figure 7a shows the shear-induced polarized light images (SIPLI) of the 3 wt% CNCs as insets, showing birefringence. At  $1 \text{ s}^{-1}$  there is an appearance of a Maltese cross, indicating a parallel orientation of one of the main axes of the optical indicatrices of a birefringent structure in the plane of polarization of the incident light. This means that the linearly polarized light passing through will not change its polarization resulting in the black sectors. For the purified CNC samples, the birefringence decreases with decreasing wt% but becomes more pronounced with increasing shear rate

(Figure S9a, Supporting Information). It is known that CNC dispersions are isotropic below a critical concentration, above which they start to enter the anisotropic chiral nematic phase showing birefringence.<sup>[78]</sup>

Figure 7b,c shows the viscosity curves for the 3 wt% aminated samples prepared from freeze-dried or evaporated material, respectively. Viscosity profiles for different wt% amine-CNC dispersions are presented in Figure S8b,c, Supporting Information. The modification of the CNCs induces a clear increase in the viscosity of the amine-CNCs (freeze-dried and evaporated), which is about 1000× that of the purified CNC dispersions (Figure 7). Once the amine-CNCs are freeze-dried, they cannot be redispersed to the same extent as the non-modified CNCs, possibly due to the strong interactions caused by opposite surface charges. Indeed, the freeze-dried sample shows aggregation and flocculation of the amine-CNCs, when imaged under non-polarized light (Figure S10, Supporting Information). However, they still formed a gel-like dispersion, where the amine-CNCs did not precipitate out of the water phase. Similar behavior for cationic CNCs has also been reported previously, even when the zeta potential is entirely positive.<sup>[79]</sup> Our amine-CNCs bear both negative and positive charges on the particle surface, which may cause irreversible flocculation and aggregation of the freeze-dried amine-CNC particles after redispersion, thus, affecting the rheological properties. To decrease the aggregation of particles induced by drying we prepared concentrated amine-CNC dispersions by evaporating the samples after modification to avoid the drying step. The viscosity of the evaporated amine-CNC dispersion (Figure 7c)

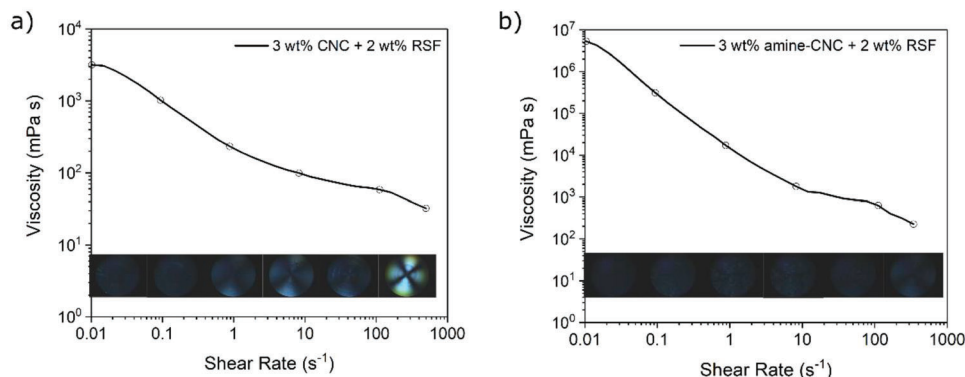


**Figure 8.** Steady-state shear viscosity curves and shear-induced polarized light images (SIPLI) as insets for a) 3 wt% cellulose nanocrystal (CNC) + 2 wt% regenerated silk fibroin (RSF) mixture, and b) 3 wt% amine-CNC + 2 wt% RSF mixture prepared from freeze-dried amine-CNCs. The circles indicate the points where the images were acquired.

remained high implying some type of ionic bridging or crosslinking between the particles even without drying the material. However, visually the evaporated dispersion was as translucent as the unmodified CNCs. In addition, the zeta potential measurements of the evaporated amine-CNCs did not show unstable behavior, which would indicate aggregation, and were similar to values of purified CNC over a wide pH range (Figure S5, Supporting Information). Furthermore, there were differences in the SIPLI images, as the SIPLI images for amine-CNCs prepared from the evaporated material showed better orientation showing an appearance of the Maltese cross (Figure 7c) compared to the freeze-dried CNCs, which showed isotropic behavior at all concentrations. This indicates that the freeze-drying of amine-CNCs prevents the formation of clear liquid crystalline phases after redispersion and that the birefringence, that is, alignment, can be better conserved when using evaporation to prepare the concentrated amine-CNC dispersions (Figure 7c). However, the birefringence was not as distinct as for the purified CNCs. The effect of wt% on the birefringence for amine-CNCs (evaporated) is presented in Figure S9b, Supporting Information.

### 3.3.2. Rheological Properties and Alignment of Mixtures of CNCs and RSF

Mixtures of the different CNCs (amine-CNCs (freeze-dried) and purified CNCs) and RSF were prepared and imaged using SIPLI. **Figure 8** shows that the addition of RSF to CNC and amine-CNC dispersions slightly increased the viscosity, as expected. Freeze-dried amine-CNCs were used for the mixtures instead of evaporated amine-CNCs as the viscosity of the evaporated amine-CNCs was already very high at 3 wt%. Thus, it was difficult to efficiently mix RSF with amine-CNCs at even higher concentrations to result in a final amine-CNC consistency of 3 wt%. The addition of RSF to CNCs did not affect the alignment of the sample and RSF seems to orientate together with the CNCs as there is a clear Maltese cross visible when imaged using SIPLI (Figure 8a). By increasing the shear rate, the birefringence becomes even more pronounced. A very light Maltese cross can be detected for the 3 wt% amine-CNC + 2 wt% RSF sample (Figure 8b), indicating some alignment is induced when combining RSF and freeze-

dried amine-CNCs. RSF on its own showed no birefringence (Figure S11, Supporting Information).

Rheological measurements and SIPLI were also conducted on the crosslinked system (Figure S12, Supporting Information). However, the high viscosity already at a low solid content prevented us from performing the crosslinking at higher wt%, similar to those of the other mixtures. In addition, the formation of clustering was observed in the SIPLI supporting the AFM images, which showed that RSF formed spherical nanostructures when adsorbing on the CNC surface. Thus, the rheology measurements and SIPLI results indicate that silk can orientate with the CNCs when not covalently bound by crosslinking. Furthermore, the CNC + RSF mixture showed the best alignment suggesting that amination is not able to increase the alignment. However, higher viscosity is beneficial in spinning experiments, which could facilitate the formation of amine-CNC + RSF composite filaments. The preliminary spinning experiments were conducted for the mixtures of CNCs (purified CNCs and amine-CNCs) and RSF and evaporated amine-CNCs were used for spinning as they did not form aggregated structures and showed better alignment in the SIPLI images.

### 3.3.3. Filament Dry-Spinning: A Preliminary Demonstration

A preliminary study was performed to show the potential of the silk and CNC composites to be used in filament spinning. Spinning experiments were performed for two mixtures: CNC+RSF and amine-CNC+RSF, as these both showed orientational behavior in the SIPLI experiments. In addition, 100% CNC, 100% amine-CNC, and 100% RSF were spun, for reference. We were able to spin both mixtures. However, the spinning of the CNC+RSF mixture was more successful than the amine-CNC+RSF as we were able to acquire higher amounts of filaments (**Figure 9**). This is supported by the SIPLI images, which showed a better orientation of the CNC+RSF than the amine-CNC+RSF mixture. The strength and strain properties of the two mixtures, however, remained quite low (Figure S13, Supporting Information) and optimization of the spinning process is still required. The amine-CNC+RSF filament's force-elongation curves showed two types of behavior. This may be originating from the



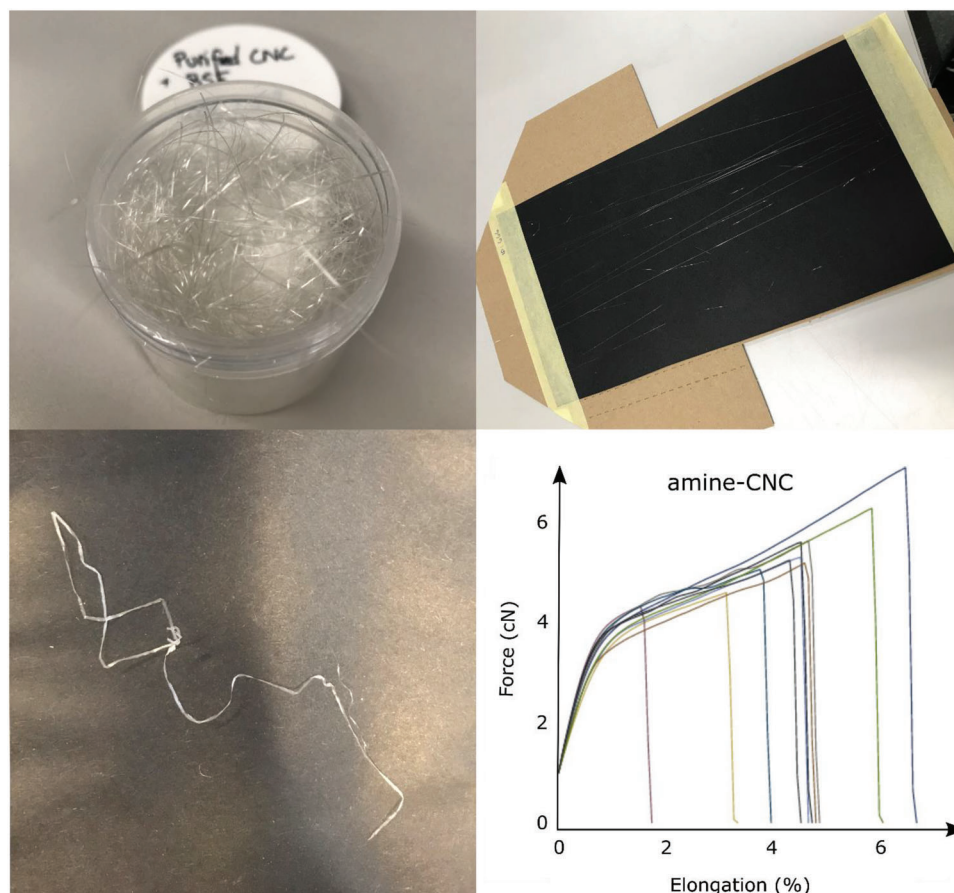


**Figure 9.** Collage of the spun cellulose-silk mixtures (upper row) and amine-modified cellulose nanocrystals (amine-CNCs) (lower row). Top left purified cellulose nanocrystals + regenerated silk fibroin (CNC+RSF), top right amine-CNC+RSF, lower left amine-CNC, and lower right force-elongation curve of amine-CNCs.

strong adhesion of the filaments (filaments were rather flat) to the substrate and once they were detached the mechanical properties were affected.

The amine-CNC dispersions' rheological properties also indicated that some type of crosslinking, either ionic or covalent, occurred between the crystallites, as the dispersion viscosities were drastically higher than that for purified CNCs. Thus, we wanted to see whether this interesting behavior would be translated into the filament properties. We were not able to spin the purified CNCs. This is due to the rod-like morphology of the crystallites and their high colloidal stability, where the high surface charge causes repulsion between the crystallites preventing aggregation.

CNCs are mostly used as strength additives in composite fibers and only a few studies have shown the successful spinning of pure CNCs.<sup>[38,39]</sup> Interestingly, we were able to spin 100% amine-CNC filaments, which showed atypical strain values at breakage for CNCs (Figure 9). Despite our efforts to reveal possible crosslinking using NMR, we were not able to show this. However, the XPS results, rheological measurements, and the strain properties of the filament strongly suggest, even if indirectly, the existence of crosslinking between the crystallites.

**Table 5,** concludes the spinning results and shows that when interactions between the components are attractive and induced by electrostatic interactions as demonstrated by QCM-D or

**Table 5.** Summary table of preliminary spinning experiments.

Sample	Interaction	Alignment under shear	Filament spinning
amine-CNC <sup>a)</sup>	attractive (rheology and XPS) <sup>b)</sup>	medium	successful
CNC + RSF	attractive (QCM-D) <sup>c)</sup>	strong	successful
amine-CNC <sup>a)</sup> + RSF	attractive (QCM-D) <sup>c)</sup>	weak	challenging
SANH-CNC + SFB-RSF	Highly attractive (QCM-D) <sup>d)</sup>	clustering, no alignment	not possible

<sup>a)</sup> Evaporated amine-CNCs; <sup>b)</sup> Attractive electrostatic interactions indirectly revealed by rheology (high viscosity) and XPS (positively charged NH<sub>3</sub><sup>+</sup> groups); <sup>c)</sup> Attractive electrostatic interactions revealed by QCM-D; <sup>d)</sup> Highly attractive due to covalent crosslinking revealed by QCM-D.

rheology and XPS measurements, and when there is clear alignment shown by SIPLI, filament spinning is most successful. In light of these results, further optimization of the spinning process, especially the spinning substrate, has to be completed to further improve the mechanical properties of the filaments, and to form round cross-sections of the filaments.

#### 4. Conclusion

In this study, we have successfully combined functionalized CNCs with silk proteins (RSF), studied the interactions between the two components, and assessed their alignment under shear. Finally, we tentatively demonstrated their applicability in filament formation. First, we were able to demonstrate the direct attachment of the amine functionality on the CNCs by using a novel liquid-state NMR approach, which is a critical factor to reduce the downstream leaching of the introduced functionalities, from the surface of the CNCs. In the QCM-D studies, we showed that RSF can interact and adsorb on both purified CNC and amine-CNC via attractive physico-chemical interactions and that the interactions did not prevent the alignment and orientation of the CNCs when mixed with RSF. However, the alignment of the amine-CNCs was not as strong as for the purified CNCs, indicating that the modification hindered the ability of the crystallites to align. Covalent crosslinking was able to increase the binding between CNCs and RSF, however, at the same time it induced the formation of protein nanoclusters on the CNCs, preventing the orientation of the system under shear. Thus, we can conclude that when non-covalent, attractive interactions are present and when the alignment of the CNCs is not strongly affected (i.e., via modification), filament spinning was most successful. These factors were fulfilled in the CNC + RSF mixture and thus it performed the best in the preliminary spinning experiments. Interestingly, we were also able to spin filaments from amine-CNCs alone. The high viscosity of the amine-CNCs indicated some type of attractive interactions taking place between the crystallites. This was supported by the XPS data, which showed that the amine-CNCs bear both positively and negatively charged domains, which could facilitate the spinning together with high viscosity and lead to atypical strain properties for CNCs.

#### Supporting Information

Supporting Information is available from the Wiley Online Library or from the author.

#### Acknowledgements

The authors thank the European Union's Horizon 2020 research and innovation program within the project "Flow Induced Phase Transitions" (713475—FLIPT—H2020-FETOPEN-2014-2015/H2020-FETOPEN-2014-2015-RIA) for financial support. In addition, this work has been done as a part of the Academy of Finland's Flagship Programme under Projects No. 318890 and 318891 (Competence Centre for Materials Bioeconomy, FinnCERES). S.A. was funded by the Academy of Finland grant #326262/311608. In addition, the authors thank Leena-Sisko Johansson for performing part of the XPS measurements.

#### Conflict of Interest

The authors declare no conflict of interest.

#### Data Availability Statement

The data that support the findings of this study are available from the corresponding author upon reasonable request.

#### Keywords

alignment, cellulose nanocrystals, interactions, regenerated silk fibroins, silanization

Received: February 22, 2023

Revised: May 2, 2023

Published online: June 4, 2023

- [1] S. Ling, W. Chen, Y. Fan, K. Zheng, K. Jin, H. Yu, M. J. Buehler, D. L. Kaplan, *Prog. Polym. Sci.* **2018**, *85*, 1.
- [2] C. Holland, F. Vollrath, A. J. Ryan, O. O. Mykhaylyk, *Adv. Mater.* **2012**, *24*, 105.
- [3] Y. Habibi, L. A. Lucia, O. J. Rojas, *Chem. Rev.* **2010**, *110*, 3479.
- [4] H. Kangas, *Opas Sellouloosa-Nanomateriaaleihin*; VTT Technology 199; Espoo, **2014**.
- [5] T. Saito, Y. Nishiyama, J. L. Putaux, M. Vignon, A. Isogai, *Biomacromolecules* **2006**, *7*, 1687.
- [6] M. Pääkko, M. Ankerfors, H. Kosonen, A. Nykänen, S. Ahola, M. Österberg, J. Ruokolainen, J. Laine, P. T. Larsson, O. Ikkala, T. Lindström, *Biomacromolecules* **2007**, *8*, 1934.
- [7] O. M. Vanderfleet, E. D. Cranston, *Nat. Rev. Mater.* **2021**, *6*, 124.
- [8] E. Kontturi, P. Laaksonen, M. B. Linder, Nonappa, A. H. G., O. J. Rojas, O. Ikkala, *Adv. Mater.* **2018**, *30*, 1703779.
- [9] NanoCrystalline Cellulose Manufacturing Expert | Celluforce, <https://celluforce.com/> (accessed: May 2023).
- [10] M. S. Reid, M. Villalobos, E. D. Cranston, *Langmuir* **2017**, *33*, 1583.
- [11] M. S. Reid, M. Villalobos, E. D. Cranston, *Nanoscale* **2016**, *8*, 12247.
- [12] J. Araki, M. Wada, S. Kuga, T. Okano, *Langmuir* **2000**, *16*, 2413.
- [13] E. Kontturi, A. Meriluoto, P. A. Penttilä, N. Baccile, J. M. Malho, A. Potthast, T. Rosenau, J. Ruokolainen, R. Serimaa, J. Laine, H. Sixta, *Angew. Chem., Int. Ed.* **2016**, *55*, 14455.
- [14] M. Lorenz, S. Sattler, M. Reza, A. Bismarck, E. Kontturi, *Faraday Discuss.* **2017**, *202*, 315.
- [15] A. Dufresne, *Mater. Today* **2013**, *16*, 220.
- [16] S. Magalhães, L. Alves, B. Medronho, A. C. Fonseca, A. Romano, J. F. J. Coelho, M. Norgren, *Polymers* **2019**, *11*, 1685.
- [17] I. Diddens, B. Murphy, M. Krisch, M. Müller, *Macromolecules* **2008**, *41*, 9755.
- [18] M. Mariano, N. El Kissi, A. Dufresne, *J. Polym. Sci., Part B: Polym. Phys.* **2014**, *52*, 791.
- [19] J. F. Revol, H. Bradford, J. Giasson, R. H. Marchessault, D. G. Gray, *Int. J. Biol. Macromol.* **1992**, *14*, 170.
- [20] S. Shafiei-Sabet, W. Y. Hamad, S. G. Hatzikiriakos, *Langmuir* **2012**, *28*, 17124.
- [21] C. Fu, Z. Shao, V. Fritz, **2009**, *2009*, 6515.
- [22] L. Nilebäck, S. Arola, M. Kvick, A. Paananen, M. B. Linder, M. Hedhammar, *Langmuir* **2018**, *34*, 11795.
- [23] S. R. Koebley, D. Thorpe, P. Pang, P. Chrisochoides, I. Greving, F. Vollrath, H. C. Schniepp, *Biomacromolecules* **2015**, *16*, 2796.
- [24] H. J. Jin, D. L. Kaplan, *Nature* **2003**, *424*, 1057.
- [25] B. Guanqiang Zhou, Z. Shao, D. P. Knight, J. Yan, X. Chen, X. Chen, G. Q. Zhou, Z. Z. Shao, J. P. Yan, D. P. Knight, *Adv. Mater.* **2009**, *21*, 366.
- [26] J. Huang, L. Liu, J. Yao, *Fibers Polym.* **2011**, *12*, 1002.
- [27] Y. Feng, X. Li, M. Li, D. Ye, Q. Zhang, R. You, W. Xu, *ACS Sustainable Chem. Eng.* **2017**, *5*, 6227.

- [28] Y. Noishiki, Y. Nishiyama, M. Wada, S. Kuga, J. Magoshi, *J. Appl. Polym. Sci.* **2002**, *86*, 3425.
- [29] L. Liu, X. Yang, H. Yu, C. Ma, J. Yao, *RSC Adv.* **2014**, *4*, 14304.
- [30] P. Dorishetty, R. Balu, S. S. Athukoralalage, T. L. Greaves, J. Mata, L. De Campo, N. Saha, A. C. W. Zannettino, N. K. Dutta, N. R. Choudhury, *ACS Sustainable Chem. Eng.* **2020**, *8*, 2375.
- [31] P. Mohammadi, A. S. Aranko, C. P. Landowski, O. Ikkala, K. Jaudzems, W. Wagermaier, M. B. Linder, *Sci. Adv.* **2019**, *5*, eaaw2541.
- [32] S. Meirovitch, Z. Shtein, T. Ben-Shalom, S. Lapidot, C. Tamburu, X. Hu, J. A. Kluge, U. Raviv, D. L. Kaplan, O. Shoseyov, *Int. J. Mol. Sci.* **2016**, *17*, 1573.
- [33] N. Mittal, R. Jansson, M. Widhe, T. Benselfelt, K. M. O. Håkansson, F. Lundell, M. Hedhammar, L. D. Söderberg, *ACS Nano* **2017**, *11*, 5148.
- [34] Z. Wang, W. Hu, Y. Du, Y. Xiao, X. Wang, S. Zhang, J. Wang, C. Mao, *ACS Appl Mater Interfaces* **2020**, *12*, 13622.
- [35] S. Arola, T. Tammelin, H. Setälä, A. Tullila, M. B. Linder, *Biomacromolecules* **2012**, *13*, 594.
- [36] A. Khakalo, T. Mäkelä, L. S. Johansson, H. Orelma, T. Tammelin, *ACS Appl. Bio Mater.* **2020**, *3*, 7428.
- [37] H. Khanjanzadeh, R. Behrooz, N. Bahramifar, W. Gindl-Altmatter, M. Bacher, M. Edler, T. Griesser, *Int. J. Biol. Macromol.* **2018**, *106*, 1288.
- [38] J. Wang, Q. Gao, Y. Wang, X. Liu, S. Nie, *Ind. Crops Prod.* **2022**, *178*, 114599.
- [39] J. Araki, M. Miyayama, *Polymer* **2020**, *188*, 122116.
- [40] T. R. Dawsey, C. L. McCormick, *J. Macromol. Sci. Polymer Rev.* **2006**, *30*, 405.
- [41] M. Labet, W. Thielemans, *Cellulose* **2011**, *18*, 607.
- [42] M. S. Peresin, K. Kammiovirta, H. Heikkinen, L. S. Johansson, J. Vartiainen, H. Setälä, M. Österberg, T. Tammelin, *Carbohydr. Polym.* **2017**, *174*, 309.
- [43] T. Koso, D. Rico del Cerro, S. Heikkinen, T. Nypelö, J. Buffiere, J. E. Perea-Buceta, A. Potthast, T. Rosenau, H. Heikkinen, H. Maaheimo, A. Isogai, I. Kilpeläinen, A. W. T. King, *Cellulose* **2020**, *27*, 7929.
- [44] A. W. T. King, V. Mäkelä, S. A. Kedzior, T. Laaksonen, G. J. Partl, S. Heikkinen, H. Koskela, H. A. Heikkinen, A. J. Holding, E. D. Cranston, I. Kilpeläinen, *Biomacromolecules* **2018**, *19*, 2708.
- [45] S. Eyley, W. Thielemans, *Nanoscale* **2014**, *6*, 7764.
- [46] A. N. Fernandes, L. H. Thomas, C. M. Altaner, P. Callow, V. T. Forsyth, D. C. Apperley, C. J. Kennedy, M. C. Jarvis, *Proc. Natl. Acad. Sci. U. S. A.* **2011**, *108*, E1195.
- [47] G. T. Hermanson, in *Bioconjugate Tech.*, Elsevier Science & Technology, Amsterdam **2013**, pp. 757–785.
- [48] P. Eronen, J. Laine, J. Ruokolainen, M. Österberg, *J. Colloid Interface Sci.* **2012**, *373*, 84.
- [49] M. Hakalahti, M. Faustini, C. Boissière, E. Kontturi, T. Tammelin, *Biomacromolecules* **2017**, *18*, 2951.
- [50] M. Rodahl, F. Höök, A. Krozer, P. Brzezinski, B. Kasemo, *Rev. Sci. Instrum.* **1995**, *66*, 3924.
- [51] I. Reviakine, D. Johannsmann, R. P. Richter, *Anal. Chem.* **2011**, *83*, 8838.
- [52] F. Höök, M. Rodahl, P. Brzezinski, B. Kasemo, *Langmuir* **1998**, *14*, 729.
- [53] O. O. Mykhaylyk, N. J. Warren, A. J. Parnell, G. Pfeifer, J. Laeuger, *J. Polym. Sci., Part B: Polym. Phys.* **2016**, *54*, 2151.
- [54] L. Völker-pop, J. Läuger, *Annu. Trans. Nord. Rheol. Soc.* **2018**, *26*, 11.
- [55] M. C. B. Salon, G. Gerbaud, M. Abdelmouleh, C. Bruzzese, S. Boufi, M. N. Belgacem, *Magn. Reson. Chem.* **2007**, *45*, 473.
- [56] L. S. Johansson, T. Tammelin, J. M. Campbell, H. Setälä, M. Österberg, *Soft Matter* **2011**, *7*, 10917.
- [57] M. Fan, D. Dai, B. Huang, in *Fourier Transform – Mater. Anal.* (Ed.: S. Salih), InTech, Rijeka, Croatia, **2012**, pp. 45–69.
- [58] P. Zhang, Y. Lu, M. Fan, P. Jiang, Y. Dong, *J. Appl. Polym. Sci.* **2019**, 48228.
- [59] E. Robles, I. Urruzola, J. Labidi, L. Serrano, *Ind. Crops Prod.* **2015**, *71*, 44.
- [60] S. C. M. Fernandes, P. Sadocco, A. Alonso-Varona, T. Palomares, A. Eceiza, A. J. D. Silvestre, I. Aki Mondragon, C. S. R. Freire, *ACS Appl. Mater. Interfaces* **2013**, *5*, 3290.
- [61] L.-S. Johansson, J. M. Campbell, *Surf. Interface Anal.* **2004**, *36*, 1018.
- [62] A. J. Varma, *Carbohydr. Polym.* **1984**, *4*, 473.
- [63] W. Thielemans, M. N. Belgacem, A. Dufresne, *Langmuir* **2006**, *22*, 4804.
- [64] A. F. d. M. Pinheiro, A. Nijmeijer, V. G. P. Sripathi, L. Winnubst, *Eur. J. Chem.* **2015**, *6*, 287.
- [65] R. M. Brown, I. M. Saxena, K. Kudlicka, *Trends Plant Sci.* **1996**, *1*, 102.
- [66] K. Wickholm, P. T. Larsson, T. Iversen, *Carbohydr. Res.* **1998**, *312*, 123.
- [67] R. H. Newman, *Solid State Nucl. Magn. Reson.* **1999**, *15*, 21.
- [68] O. M. Terrett, J. J. Lyczakowski, L. Yu, D. Iuga, W. T. Franks, S. P. Brown, R. Dupree, P. Dupree, *Nat. Commun.* **2019**, *10*, 4978.
- [69] J. D. Kubicki, H. Yang, D. Sawada, H. O'Neill, D. Oehme, D. Cosgrove, *Sci. Rep.* **2018**, *8*, 13983.
- [70] K. Daicho, T. Saito, S. Fujisawa, A. Isogai, *ACS Appl. Nano Mater.* **2018**, *1*, 5774.
- [71] D. P. Oehme, M. T. Downton, M. S. Doblin, J. Wagner, M. J. Gidley, A. Bacic, *Plant Physiol.* **2015**, *168*, 3.
- [72] T. Rosén, H. R. He, R. Wang, C. Zhan, S. Chodankar, A. Fall, C. Aulin, P. T. Larsson, T. Lindström, B. S. Hsiao, *ACS Nano* **2020**, *14*, 16743.
- [73] J. Sugiyama, R. Vuong, H. Chanzy, *Macromolecules* **1991**, *24*, 4168.
- [74] T. G. Parton, R. M. Parker, G. T. van de Kerkhof, A. Narkevicius, J. S. Haataja, B. Frka-Petesic, S. Vignolini, *Nat. Commun.* **2022**, *13*, 2657.
- [75] A. Aguilar-Sanchez, B. Jalvo, A. Mautner, S. Nameer, T. Pöhler, T. Tammelin, A. P. Mathew, *J. Memb. Sci.* **2021**, *620*, 118842.
- [76] L. Bai, Y. Liu, A. Ding, N. Ren, G. Li, H. Liang, *Chemosphere* **2019**, *217*, 76.
- [77] S. Shafeiei-Sabet, W. Y. Hamad, S. G. Hatzikiriakos, *Rheol. Acta* **2013**, *52*, 741.
- [78] S. Beck-Candanedo, M. Roman, D. G. Gray, *Biomacromolecules* **2005**, *6*, 1048.
- [79] M. S. Reid, S. A. Kedzior, M. Villalobos, E. D. Cranston, *Langmuir* **2017**, *33*, 7403.